Materials for Small-Scale Space Propulsion Systems

by

Alexander Connor Larkin Bost

B.S., Mechanical Engineering, Lehigh University (2009)

Submitted to the Department of Aeronautics and Astronautics
in partial fulfillment of the requirements for the degree of

Master of Science in Aeronautics and Astronautics

at the

MASSACHUSETTS INSTITUTE OF TECHNOLOGY

June 2017

© Massachusetts Institute of Technology 2017. All rights reserved.

Signature redacted

Author ....
Department of Aeronautics and Astronautics
May 25, 2017

Signature redacted

Certified by ....
Paulo C. Lozano
Associate Professor
Thesis Supervisor

Signature redacted

Accepted by ....
Youssef M. Marzouk
Associate Professor of Aeronautics and Astronautics
Chair, Graduate Program Committee

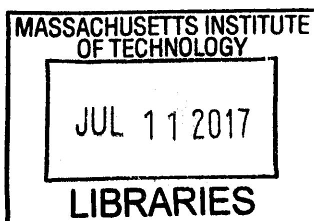
MASSACHUSETTS INSTITUTE OF TECHNOLOGY
JUL 11 2017
LIBRARIES
ARCHIVES

Materials for Small-Scale Space Propulsion Systems

by

Alexander Connor Larkin Bost

Submitted to the Department of Aeronautics and Astronautics
on May 25, 2017, in partial fulfillment of the
requirements for the degree of
Master of Science in Aeronautics and Astronautics

Abstract

This thesis explores a variety of materials and methods for creating emitter arrays for the ion electrospray propulsion system (iEPS), a compact, efficient, and scalable space propulsion system for use in a wide range of space missions. The increasing utilization of small, cheap, easy-to-launch satellites known as CubeSats has spurred demand for a propulsion system which exists at the nexus of high power efficiency, low mass, surface area, and volume, and high specific impulse. iEPS has demonstrated a unique potential to satisfy all of these stringent design requirements in a way no presently existing propulsion system can.

The first part of this work explores utilizing microelectromechanical systems (MEMS) processing to increase the thrust density of iEPS. Silicon molds were designed and manufactured with differing emission site size and spacing. Additionally, a variety of materials were tested with the aim of forming a porous network within the molds prior to selective removal of the mold. A molded array is successfully fired as a result of these research efforts.

The second part of this work explores creation of porous substrates for use with an existing laser ablation method of creating emitter arrays. The first iEPS thrusters tested in space used porous borosilicate glass emitter chips, which demonstrated shortcomings in terms of material uniformity, pore size, and ionic liquid fuel containment. This work explores materials and methods for improving all of these and demonstrates the successful firing of an array made by sintering a silicon dioxide nano-bead powder.

Thesis Supervisor: Paulo C. Lozano
Title: Associate Professor

Acknowledgments

This work was funded by MIT Lincoln Labs and the U.S. Government.

Many of the opportunities I've had, which allowed me to go from working at a gym to becoming an MIT rocket scientist, have come from others going out on a limb for me. I owe a great deal to Professors Krystyn Van Vliet and Sebastian Seung for giving me my first chance to work in academic research back in 2011 when I had no research experience to speak of. Similarly for Professor Ray Ashoori and the rest of the Ashoori Group, Ben Hunt and Andrea Young especially, for letting me wander into the lab and start soldering things. And to any number of grad students who took the time to sit down and chat with me about research over coffee before I became a grad student, like Javier Sanchez-Yamagishi and Tom Coles, thank you.

Of those to whom I am indebted at MIT, few deserve more thanks than Paulo Lozano, my advisor. I still remember meeting with him for the first time and proposing he let me help out with research here and there; describing his reaction as skeptical would be an understatement. Yet, somehow, I convinced him to let me start helping out and that was good enough for me. Paulo is one of the most relentlessly optimistic people I know, and genuinely cares for the people with whom he works. I have benefited directly from that over and over again.

I have many thanks to give to my lab mates in the SPL. To Louis Perna especially, who has always been willing to help with MTL processes, LaTeX questions, where I can find something in the lab, anything at all. His assistance has saved me hours of frustration, and I am extremely grateful to have had someone so unfailingly generous as a resource during my time with the SPL. To my lab and office mate Dakota Freeman, who has been one of the first people in the lab I turn to to bounce ideas off of, as well as a source of excellent conversations throughout my time as a grad student. I'm happy to report that no working hours were lost to political discussion during our time sharing an office. To David Krejci for his help and hard work in the

lab, especially performing the testing of the SiO_2 emitter array detailed in this work. I also owe him for getting me to give windsurfing a try instead of spending all my time in sailboats.

The staff of the MIT MTL were universally helpful and knowledgeable on all matters MEMS related. They are some of the best in any research lab at MIT, and I owe a great deal to them for their assistance during my entire time in the MTL. To Dennis, Kurt, Gary, Donal, and everyone else, thank you.

To my Burton Third Bombers, who have been exemplars of responsibility and maturity to the entire MIT undergraduate community for 333rd years. a btb "I will remember the floor always, or for 3rd years, whichever comes first" comm.prod.

Setting aside time for personal pursuits is hard at MIT, but I'm lucky to have been a part of the MIT Sailing Team and Club Hockey Team, which helped me keep my sanity more or less intact while I was a student. Thank you to Technique as well, for letting me use camera equipment that probably exceeded my net worth, and more importantly, to the people in all of these groups.

To my half-sister Anne, for giving me one less thing to worry about when I was folding towels at the start of my not-so-promising career.

And lastly, to my family. I could not have overcome the challenges I did if I hadn't had a rock solid foundation to work from, and for that I am forever grateful.

Contents

1 Introduction **17**

1.1 Fundamentals of Rocket Propulsion 17

1.2 Ion Electrospray Propulsion 28

1.3 Present State of the Art and Main Challenges 32

2 Array Molding and Fabrication **35**

2.1 Mold Design and Fabrication 35

2.2 Materials Testing 38

2.2.1 Sintering 38

2.2.2 Soda-Lime Glass Beads 39

2.2.3 Xerogels 42

2.2.4 Silicon Dioxide (SiO_2) Micro-Spheres 44

2.3 Production of Arrays 46

3 SiO_2 Array Fabrication **49**

3.1 Current Methods and Challenges 49

3.2 Hydraulic Pressing of Emitter Chips 54

3.2.1 Method 54

3.2.2 Alternate Mixtures and Furnace Recipes 59

3.3 Laser Ablation of SiO_2 Emitter Chips 65

3.3.1 First Laser Ablation 65

3.3.2 Laser Parameter Variation for Emitter Refinement 68

4 Test Results **75**

4.1 Si Mold Array 75

4.1.1 Current vs. Voltage Plot 77

4.1.2 Trapezoidal Voltage Waveform 78

4.2 SiO_2 Nano-Bead Array 78

4.2.1 Current vs. Voltage Plot 79

4.2.2 Retarding Potential Analysis 80

4.2.3 Trapezoidal Voltage Waveform 83

5 Summary and Future Research Directions **85**

5.1 Array Molding 86

5.2 SiO_2 Emitter Arrays 87

5.3 Future Research Directions 88

5.3.1 Array Molding 88

5.3.2 SiO_2 Emitter Arrays 89

5.4 Conclusion 89

List of Figures

1-1 A rocket enclosed by a control volume [1]. 19

1-2 Chemical propulsion Δv vs m_0/m_f 21

1-3 An ion in an electric potential. 22

1-4 Chemical and electric propulsion Δv vs m_0/m_f 24

1-5 The NASA/JPL NEXIS Ion Thruster [2]. 27

1-6 A Busek BHT-8000 Hall thruster [3]. 27

1-7 Top down view of tip array aligned to extractor grid holes. 29

1-8 iEPS frame, emitter, and extractor. 30

1-9 Assembled iEPS thruster package. 30

1-10 CAD models of iEPS 2.2F 30

2-1 MEMS processing steps for creating the Si molds. 36

2-2 Wafer with outlines of individual mold dies. 37

2-3 A diagram of the sintering process [4]. 39

2-4 SEM image of soda-lime glass beads after sintering. 40

2-5 Sintering profile vs. time in hours. 41

2-6 Non-porous skin on outer surface of RF substrate material. 43

2-7 RF etched by RIE plasma. 43

2-8 RF after etching in TMAH. No RF remains. 43

2-9 2 µm SiO_2 microbeads in a mold channel. 44

2-10 SiO_2 micro-spheres coated and bound using soda-lime nano-spheres. . 45

2-11 A cluster of partially-etched emitters. 45

2-12 A single 57 µm diameter soda-lime glass emitter after mold etching. . 46

2-13 225 µm pitch array after approximately 50 µm of etching. 46

2-14 A 48 µm diameter column after 83 µm of etching. 47

2-15 A single 38 µm column. 47

2-16 Side view of an array after part of the etching process. 47

2-17 Array of soda-lime emitters after mold etching. 47

2-18 450 μm pitch array filled with EMI-BF_4 ionic liquid. 48

2-19 A 225 µm array of 43 µm cylinders filled with ionic liquid. 48

2-20 A single 43 µm tip from a 225 µm pitch array filled with ionic liquid. 48

3-1 SEM of a borosilicate chip used to fabricate emitters. 50

3-2 Image of pooling phenomenon. 50

3-3 Diagram illustrating ionic liquid creep. 51

3-5 Unpacked SiO_2 beads sintered at 1250 °C 55

3-6 Pressing die 56

3-7 Hydraulic press 56

3-8 Layering in SiO_2 chip 56

3-9 Sintered SiO_2 57

3-10 Post-sintered SiO_2 chip 57

3-11 Layering in SiO_2 chip 58

3-12 Increased sintering in CO_2 flow 62

3-13 SiO_2 chips after sintering in CO_2 flow 62

3-14 Layering in SiO_2 chip 64

3-15 SiO_2 chips dry pressed at 5400 psig 65

3-16 First tips laser etched into SiO_2 66

3-17 Same emitter with and without ionic liquid 67

3-18 800x SEM of SIO_2 chip with ionic liquid 67

3-19 30x SEM of SIO_2 chip with ionic liquid 68

3-20 SiO_2 ablation results with varying laser parameters 69

3-21 Full 480 emitter pattern in SiO_2 chip 71

3-22 SEM comparison, laser etched borosilicate vs. SiO_2 arrays 72

3-23 SEM of laser-etched SiO_2 saturated with ionic liquid 73

4-1 Soda-lime glass array in Si mold 76

4-2 Molded soda-lime glass array seen through extractor 76

4-3 Voltage vs. current from molded soda-lime glass array. 77

4-4 Emitted current from molded soda-lime glass array. 78

4-5 SiO_2 array on test mount, current (µA) vs. voltage (V) 79

4-6 Diagram of a retarding potential anaylzer 80

4-7 RPA output for pure ionic regime 81

4-8 RPA output for single species fragmentation 82

4-9 RPA output from SiO_2 emitter array filled with EMI-Im 83

4-10 Trapezoidal voltage waveform applied to SiO_2 emitter 84

List of Tables

2.1 Si mold die specifications. 37

2.2 Table of steps in the mold fabrication process. 38

2.3 Steps to make RF xerogel. 42

2.4 Steps to make titania xerogel. 42

3.1 SiO_2 porous chip fabrication steps 58

3.2 Alternate attempted recipes for making SiO_2 chips. 60

Chapter 1

Introduction

The idea of rocket propulsion – accelerating an object to high velocity by shooting something out the back of it at a much higher velocity – has been around for hundreds of years, first exploited by the Chinese in the 13th century as a means of launching "fire arrows"[5]. The Germans played a large role in developing the field of rocket science during World War II, and following the war this expertise was utilized and expanded upon by the United States and the Soviet Union as the Cold War ramped up. This ultimately lead to the dawn of the Space Age with the launch of Sputnik 1, the world's first artificial satellite, by the Soviet Union on October 4, 1957. Billions of dollars (and rubles) were poured into researching how to launch bigger and more complex payloads into space from the surface of the Earth, and a fairly detailed understanding of the capabilities and limitations of chemical rocket propulsion was soon developed.

1.1 Fundamentals of Rocket Propulsion

The basic operating principle of rocket propulsion is fairly simple to understand. When you blow up a balloon and let it go without tying the end, it zooms through

the air because the air inside the balloon is forced out the back with some velocity and the balloon is pushed forward by the equal but opposite reaction. Chemical rockets essentially work by igniting fuel and oxygen in a combustion chamber which results in a product gas at much higher temperature and pressure, and then letting that gas escape in a (more or less) single direction. Let's imagine two identical rockets, A and B, with the exact same amount of propellant (and let's imagine that they're really far out in the middle of space so we don't have to worry about gravity or anything else pushing or pulling on them). If the propellant in rocket B shoots out twice as fast as the propellant in rocket A, this means that rocket B can eventually move twice as fast as rocket A once both have used up all of their propellant. How fast the propellant leaves the rocket (the exhaust velocity) turns out to be one of the most important factors in the performance of a rocket propulsion system. The following section will give a better understanding of other important factors, but as a general rule, the faster the propellant exhaust velocity, the more useful the rocket can ultimately be. This can translate to larger transported payloads, greater distances traveled, and/or a wider range of achievable missions.

It helps to take a look at the math and physics that underpin rocket science. Figure 1-1 shows a rocket and all of its propellant inside of a control volume. Here we assume that the rocket, like rockets A and B, is so far away from anything as to not be affected by other forces such as gravity, radiation pressure, and so on. We also assume that the control volume expands such that every atom and molecule which was in the control volume at the start is enclosed even after the rocket and its exhaust have begun moving apart at high velocities. By doing this, we can consider the total momentum of the system, $P(t)$, which will not change as the rocket begins operation, thanks to conservation of momentum. If the total momentum of the system doesn't change ($\frac{dP}{dt} = 0$), what can that tell us about the rocket? Well, in fact, this can give us quite a bit of information about how the rocket and exhaust affect and relate to each other. In Figure 1-1 $v(t)$ is the rocket velocity, $m(t)$ is the mass of the rocket (which includes propellant mass until it leaves as exhaust), $c(t)$ is the exhaust velocity, and

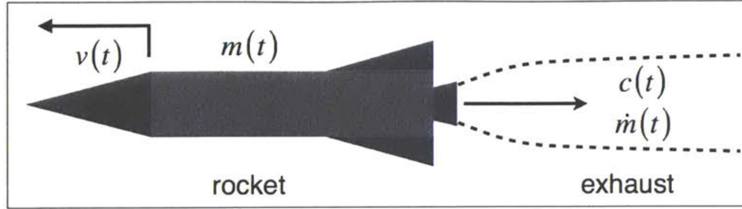

Figure 1-1: A rocket enclosed by a control volume [1].

$\dot{m}(t)$ is the mass flow rate of the exhaust. We write all of these as a function of time even though $c(t)$ and $\dot{m}(t)$ will remain constant in this example.

Let's take a look at what comprises the total momentum of the system:

$$P(t) = m(t)v(t) + \int_0^t \dot{m}(t')[v(t') - c(t')]dt' \tag{1.1}$$

It is more illuminating to examine the change of momentum of the system and each of the constituent components (the ever-lightening rocket and ever-growing exhaust plume). Since the control boundary is expanding to encapsulate all of the mass initially in the system, no external forces are acting on the system, and momentum within such a system is conserved, the momentum of the system doesn't change with time as we noted before: $\frac{dP}{dt} = 0$. Taking the derivative of equation 1.1 with respect to time, we get:

$$\frac{dP(t)}{dt} = \frac{dm(t)}{dt}v(t) + m(t)\frac{dv(t)}{dt} + \dot{m}(t)[v(t) - c(t)] = 0 \tag{1.2}$$

$\frac{dm(t)}{dt}$ is equal but opposite to the mass flow rate of the exhaust, so we can rewrite $\dot{m}$(t) as $-dm(t)/dt$. This gives:

$$\frac{dm(t)}{dt}v(t) + m(t)\frac{dv(t)}{dt} - \frac{dm(t)}{dt}[v(t) - c(t)] = 0 \tag{1.3}$$

allowing us to cancel the two $\frac{dm(t)}{dt}v(t)$ terms, and a bit of algebra gives us:

$$-\frac{dv(t)}{c} = \frac{dm(t)}{m} \tag{1.4}$$

Integrating, writing $v_f - v_0$ as Δv, and rearranging, we get the famous Tsiolkovsky rocket equation:

$$\Delta v = c \cdot ln\left(\frac{m_0}{m_f}\right) \tag{1.5}$$

Where m_0 is the total starting mass of the rocket and m_f is the mass of the rocket after firing. The exhaust velocity c is sometimes divided by the gravitational constant to give specific impulse: $I_{sp} = c/g$. I_{sp} has units of seconds and is used as an alternate measure of propulsion system performance. What the rocket equation tells us is that the change in velocity of our rocket is equal to the exhaust velocity of the propellant times the natural log of the rocket mass when we start firing the engine divided by the mass when we've finished firing the engine. In practical terms, this means that doubling the amount of propellant you have doesn't double the maximum velocity of your rocket. This makes intuitive sense: if you have a lot of propellant to start with you can fire for a longer period of time, but your rocket is heavier initially. If you cut down on the amount of propellant you have, your rocket is lighter, but you can't accelerate for as much time. Either way, carrying more propellant isn't necessarily the best way to get your rocket to go faster; having a higher exhaust velocity is. This is illustrated in figure 1.5

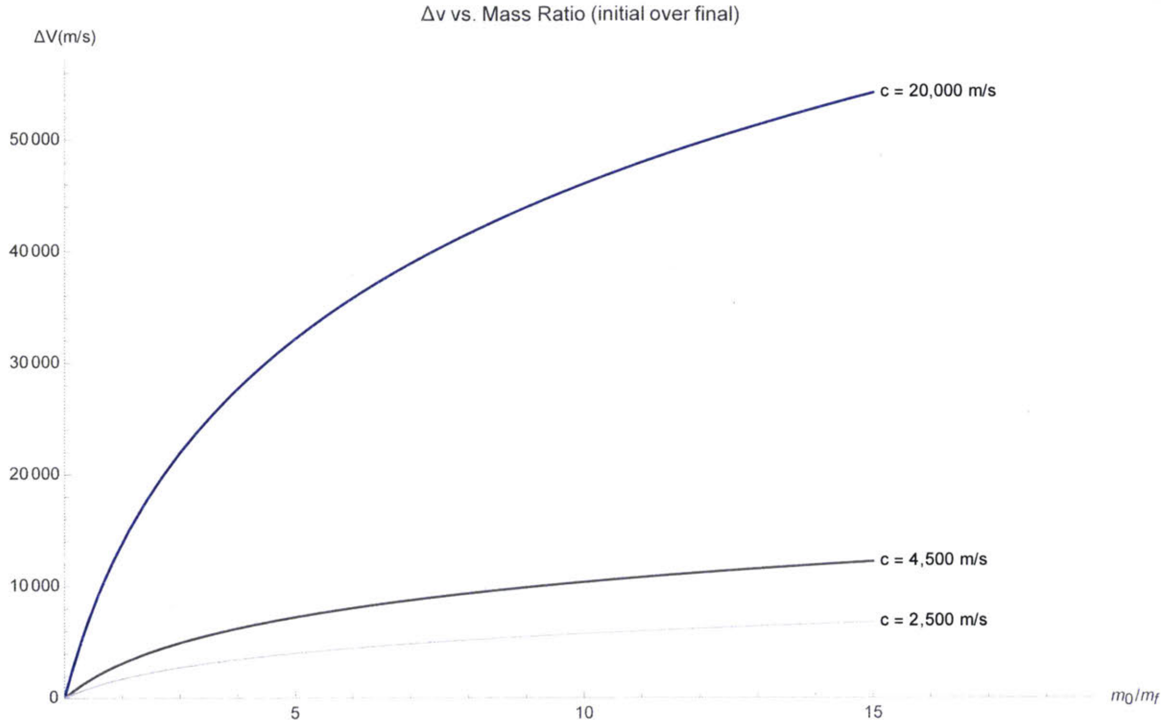

Figure 1-2: Achievable Δv vs m_0/m_f for a given exhaust velocity c. Shown are the typical upper and lower values for chemical rockets, as well as the approximate theoretical maximum achievable for chemical rockets.

We note that $m_0 - m_f = m_p$, where m_p is the propellant mass and $100 \times \left(\frac{m_0 - m_f}{m_0}\right) = 100 \times \left(\frac{m_p}{m_0}\right)$ is the mass percentage of the rocket which is propellant.

Chemical rocket engines and motors like those used on the Space Shuttle tend to have an exhaust velocity somewhere between 2,000-4,500 m/s (about 70-150 times faster than a car on the highway), and for those propulsion systems this is pretty close to as good as it gets. (The theoretical maximum comes from combining hydrogen atoms to make H_2 molecules, which results in an exhaust velocity of around 20,000 m/s; unfortunately, storing atomic Hydrogen is not currently possible.) Going back to our example with rockets A and B, we can think about how increased exhaust velocity is useful in another way: if, instead of accelerating rocket B to twice the velocity of rocket A, we want to accelerate the two rockets to the same velocity, rocket B can have almost 65% more mass dedicated to things that aren't propellant (e.g. crew, food, batteries, equipment, etc.). Rocket scientists naturally wondered

if there were other types of propulsion systems that could accelerate propellant to greater velocities and it turns out that indeed there are: electric propulsion systems.

Electric propulsion works by taking charged particles and placing them in an electric field. The particles feel a force based on the strength and direction of the electric field and accelerate accordingly. To get a better understanding of the difference between chemical and electric propulsion, let's start with the Space Shuttle Main Engine (SSME) as an example. The SSME combines hydrogen and oxygen to form water ($2H_2 + O_2 \rightarrow 2H_2O$, though other molecules show up during actual operation), and those water molecules reach velocities of close to 4,500 m/s as noted earlier. If we could ionize a water molecule and accelerate it in an electric field, what kind of voltage would we need?

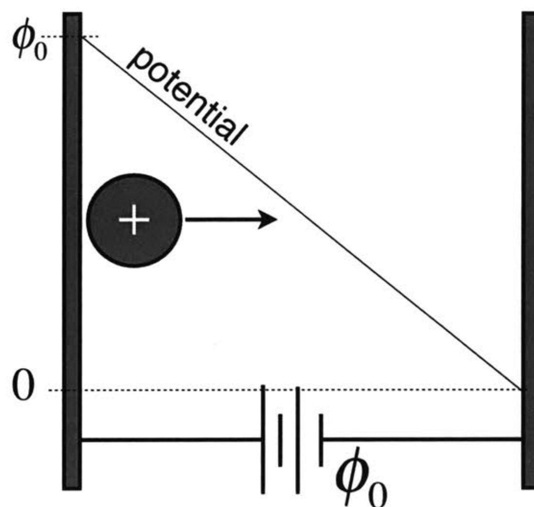

Figure 1-3: An ion in an electric potential. The charged water molecule is represented by the circle with a plus in it [1].

By applying a voltage between the two plates, we create an electric field which accelerates the molecule through the electric potential. We can use an energy balance to relate electric potential energy and kinetic energy to figure out how much voltage we would need to apply to get our water molecule to an equally high velocity as it would have when it exited the SSME. Neglecting space charge effects:

$$\frac{1}{2}m_i u_0^2 + q\phi_0 = \frac{1}{2}m_i u_1^2 + q\phi_1 \tag{1.6}$$

Where m is the ion mass, u is the ion velocity, and ϕ is the potential at a given spot between the plates. The ion starts from rest on the left, so u_0 is zero, and similarly ϕ_1 falls to zero on the right, so we have:

$$\cancel{\frac{1}{2}m_i u_0^2} + q\phi_0 = \frac{1}{2}m_i u_1^2 + \cancel{q\phi_1} \tag{1.7}$$

thus:

$$u_1 = \sqrt{\frac{2q\phi_0}{m_i}} \tag{1.8}$$

or equivalently

$$\phi_0 = \frac{m_i u_1^2}{2q} \tag{1.9}$$

So this tells us the velocity of an ion accelerated through a potential is the square root of 2 times the elementary charge e and the potential ϕ_0 divided by the mass of the ion, m_i. If our goal is to accelerate this ion to 4,500 m/s, what kind of voltage do we need for ϕ_0? With m_i = 2.99e^{-26} kg, q = 1.60e^{-19} C, and u_1 = 4,500 m/s, we find that we only need a voltage of 1.89 V, about six times lower than a typical car battery. Any increase in the voltage leads to a square root increase in the velocity: quadruple the voltage to roughly 8 V and your exhaust velocity doubles. Increase it to 200 V and exhaust velocity now goes up by more than a factor of 10. Commonly used electric propulsion systems like ion and Hall thrusters typically use voltages in the range of 300 – 8,000 V, and exhaust velocities in excess of 80,000 m/s are possible. The most powerful electric propulsion systems such as Magnetoplasmadynamic (MPD) thrusters and the Variable Specific Impulse Magnetoplasma Rocket (VASIMR) can theoretically achieve exhaust velocities higher than 100,000 m/s.

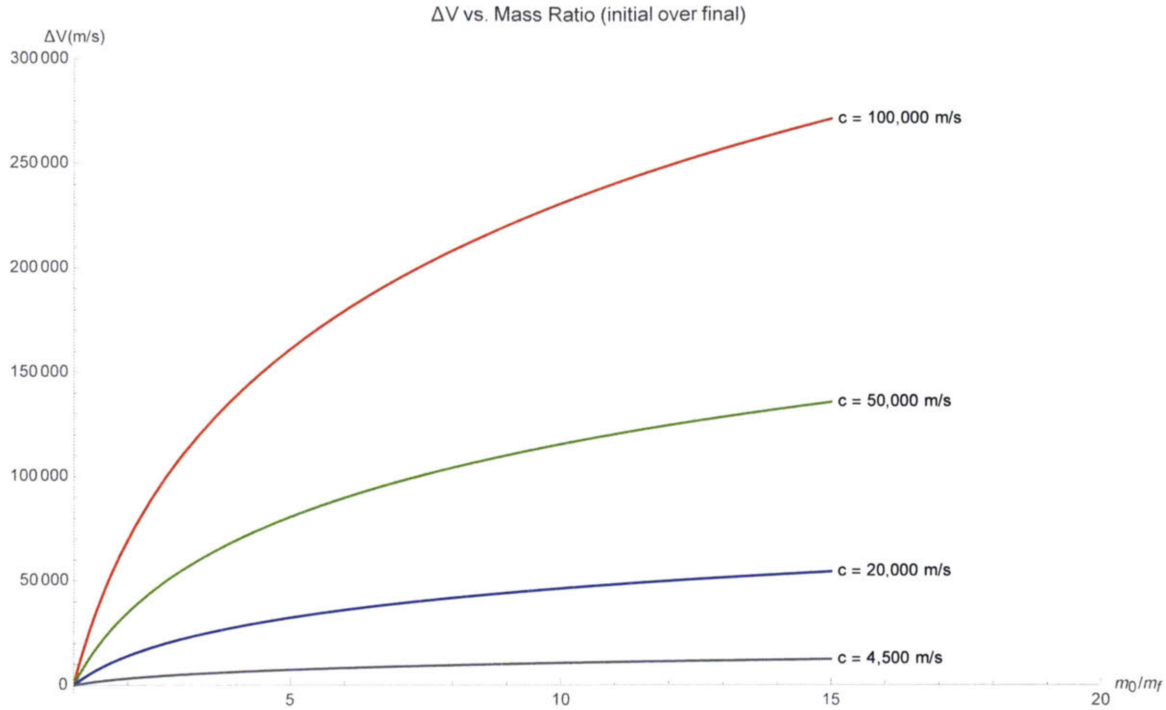

Figure 1-4: Achievable Δv vs m_0/m_f for a given exhaust velocity c ranging from 4,500 m/s (high end for chemical rockets) to 100,000 m/s (high end for electric propulsion).

Exhaust velocity isn't the only aspect of propulsion that matters, however; after all it would be pretty hard to get into space if your rocket didn't provide enough thrust to lift it off the ground. From basic physics, we know that $F = m/a = m\frac{dv}{dt}$ where $\frac{dv}{dt}$ is the same as the instantaneous acceleration a, and lurking in equations 1.3 and 1.4 we can find:

$$m\frac{dv}{dt} = -c\frac{dm}{dt} = c \cdot \dot{m}(t) \tag{1.10}$$

Which tells us that the amount of thrust a rocket produces is equal to its exhaust velocity times the mass flow rate of the exhaust. We also need to know how much power is required to accelerate a mass flow rate of propellant to a certain velocity, and these are related in the following way:

$$\mathcal{P} = \frac{\dot{m}c^2}{2\eta} \tag{1.11}$$

Where η is the efficiency of your propulsion and power system at converting stored energy to kinetic energy of the exhaust. This is one of the main differences between chemical and electric propulsion: the power source. In chemical propulsion systems, the energy to heat and pressurize the propellant in the combustion chamber is stored in the bonds of the fuel and oxygen molecules. This is convenient because the mass dedicated to propellant is simultaneously mass dedicated to the "power supply." With electric propulsion, however, the power supply is separate from the propellant which both adds complexity and decreases available mass and space for mission-related systems and payloads. This also partially explains why chemical rockets are needed to do "heavy lifting" missions, especially launching from the surface of Earth (or other heavenly body).

To see why, let's look at how much power it takes to launch a rocket. We'll use the F-1 engine of the Saturn V rocket which carried the first American astronauts to the Moon and is still one of the most powerful liquid propellant rocket engines ever made. A single F-1 engine (the Saturn V had – wait for it – five) consumed just over 670 gallons of fuel and oxidizer *per second* during operation which corresponds to an $\dot{m}$ of approximately 2576 kg/s [6]. For perspective, that's enough to fill a large back-yard pool in about a minute. With an I_{sp} of 260 seconds, corresponding to a c of $260 \cdot 9.81 = 2{,}550$ m/s, and an η of 0.9, for each engine we get $\mathcal{P} = \frac{2576 \cdot (2550)^2}{2 \cdot 0.9} = 8.375$ gigawatts. Multiply that by the five engines and that gives us a total of almost *42 gigawatts*. For comparison, the Hoover Dam can produce just over 2 gigawatts of power at maximum output, so the Saturn V effectively produced a staggering 21 Hoover Dams worth of power during first stage ascent.

Because all of the energy used to launch the Saturn V was in the bonds of the fuel and oxidizer molecules, it didn't need an external power source. However, electric propulsion systems don't have that luxury, and in general, power plants which

can produce even a fraction of the power produced by the Saturn V are the size of buildings. What this ultimately means for electric propulsion systems is that they have to trade off thrust force for exhaust velocity (and, in a sense, "fuel efficiency"). This can be seen if we rewrite equation 1.11 by noting that $F = \dot{m}c$:

$$\mathcal{P} = \frac{Fc}{2\eta} \tag{1.12}$$

Once you install a particular power system on your satellite, the amount of power you have available is fixed. So, if you want to increase the amount of thrust you get from your propulsion system, your propellant exhaust velocity will have to decrease and vice versa. As an example, let's say a typical power system on a modern satellite can produce about 5,000 W. If our exhaust velocity is 30,000 m/s and we assume a (pretty ambitious) overall efficiency of 0.9, we get a thrust force of 0.3 Newtons. This is roughly the force you would feel if you held six nickels in your hand! Here we see the trade-off of electric propulsion: you can ultimately get your rocket to higher velocities with electric propulsion, but you'll have to fire your propulsion system for *much* longer periods of time to do it. This means days or months of firing instead of seconds or minutes, which can mean longer missions.

Still, there are certain types of missions which don't suffer from increased duration or actually benefit more from low-thrust continuous firing instead of high-thrust, pseudo-impulsive firing. For example, in Low Earth Orbit (LEO) where the International Space Station (ISS) and other satellites orbit, there are a small-but-not-insignificant number of gas molecules present which create a slight drag on orbiting bodies. If these satellites don't have any on-board propulsion, they will eventually slow down enough that they will fall back into Earth's atmosphere and disintegrate upon re-entry. To counter this, the propulsion systems on these satellites are occasionally fired to give them a velocity boost and maintain their orbital altitude – a maneuver known as "station keeping." If, instead of doing all of the thrusting at once with a low-specific-impulse propulsion system like a chemical rocket, the satel-

lites make use of high-specific-impulse electric propulsion, less propellant is needed which leaves more mass available for other systems. For missions requiring high Δv, using electric propulsion results in missions that take the same amount of time as if they used chemical propulsion. And in some cases, missions are only possible by using electric propulsion instead of chemical propulsion; the NASA Dawn mission, for example.

The ion engines and Hall thrusters mentioned earlier have been around since the 1960s and have become more commonplace recently due to advances in durability and lifetime. Both of these thrusters work by ionizing a propellant gas (usually a noble gas like xenon due to its relatively high mass and low ionization potential) and accelerating the ions in an electric field. The resulting exhaust velocities are much higher than for chemical rockets, but these propulsion systems come with downsides as well. As noted earlier, the power for these propulsion systems must come from an outside source instead of from the molecules of propellant themselves as is the case with chemical rockets.

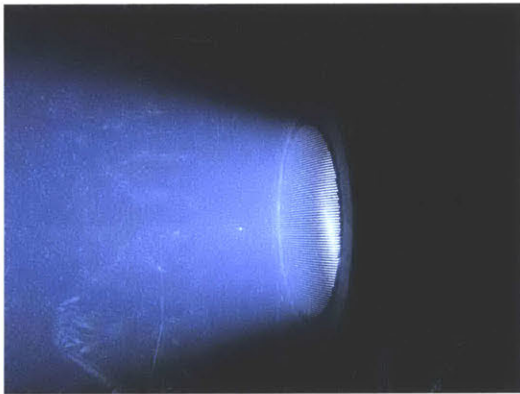

Figure 1-5: The NASA/JPL NEXIS Ion Thruster [2].

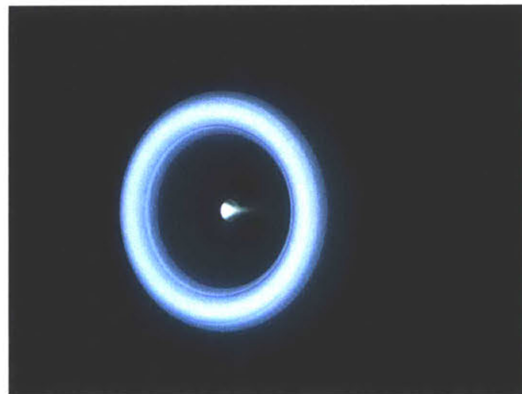

Figure 1-6: A Busek BHT-8000 Hall thruster [3].

These electric propulsion systems suffer from various efficiency losses including ionization cost, ions which hit part of the thruster and fail to escape (referred to as intercepted current), electrical losses in the power system itself, additional electrical systems required to mitigate spacecraft charging, and propellant that isn't ionized and therefore not accelerated to high velocity among others. These inefficiencies tend

to increase markedly as the size of the thruster decreases, which is particularly notable in the context of the growing popularity of microsatellites known as CubeSats.

CubeSats are small satellites that tend to come in multiples of a standard 1000 cm^3 unit or U; for instance a 6U CubeSat will have a volume of 6000 cm^3. The size of these satellites is a great advantage in terms of launch cost and accessibility; where a 4-ton satellite might have cost $300 million to launch on the Space Shuttle, CubeSats can be developed and launched for less than $100,000. This makes them highly accessible to university laboratories and small companies instead of just governments and large corporations.

With the expanding popularity of these satellites comes a need for propulsion systems which can fit into the limited packaging as well as efficiently utilize both power and propellant. Traditional chemical and electric propulsion systems have so far been unable to occupy the intersection between these design constraints, but a different type of electric propulsion known as ion electrospray propulsion has shown a promising ability to address all of these challenges.

1.2 Ion Electrospray Propulsion

Ion electrospray propulsion works by applying an electric field to an ionic liquid propellant, which has flowed to the tip of either a capillary or porous tip structure (usually 15-20 μm in radius). Upon exposure to a critical electric field strength, the liquid at the tip is stressed into a conical shape characterized by G.I Taylor and subsequently known as a Taylor Cone [7]. The conical shape further amplifies the electric field strength at the tip of the liquid cone and when it is further increased, will begin to pull individual ions or charged droplets away from the liquid to be accelerated. The ionic liquid propellants are molten salts at room temperature, consist almost purely of ions (as opposed to ions dissolved in a solvent, e.g. salt in water), and perhaps most importantly, have negligible vapor pressure. This means that the

propellant does not evaporate when exposed to the vacuum of space. Individual ions or charged droplets of propellant are pulled from the tip of the surface and accelerated through a grid whose holes have been aligned to each of the emitters as shown in Figure 1-7.

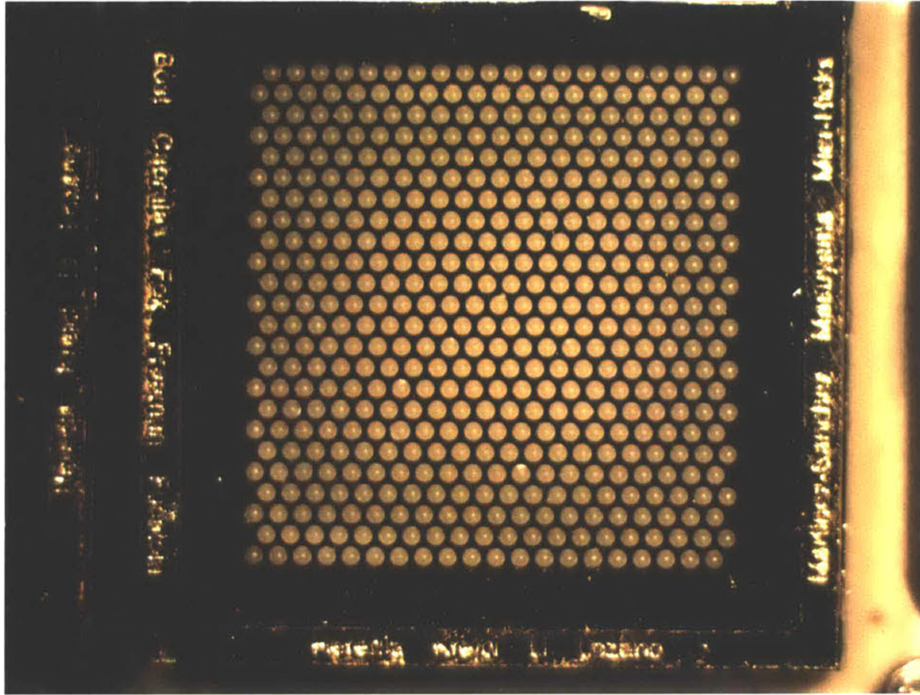

Figure 1-7: Top down view of tip array aligned to extractor grid holes. The grid holes are 300 µm in diameter and arranged in a staggered 24 x 20 array. Each hole and tip is spaced 450 µm from its neighbors in a hexagonal pattern.

The MIT Space Propulsion Lab (SPL) principal research focus is the ion electrospray propulsion system (iEPS), a small, scalable, efficient implementation of electrospray propulsion in a package smaller than a quarter.

To give a sense of scale, the iEPS components in Figures 1-8 and 1-9 are on a glass slide 1" wide by 3" long. This packaging system was originally developed by Robert Legge [8] and Daniel Courtney [9] as part of their Ph.D. work and further developed by Louis Perna [10] during his Master's thesis work. This packaging utilizes microelectromechanical systems (MEMS) processing technology to create features with nano-scale precision as well as to increase throughput by creating the Si packaging in

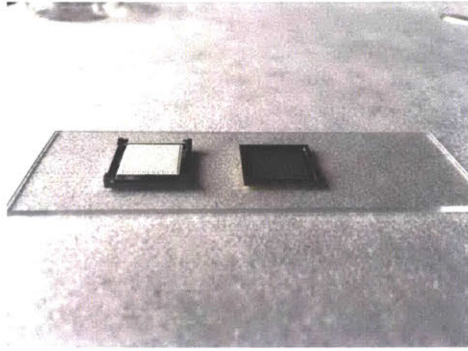

Figure 1-8: An iEPS emitter chip mounted on the silicon (Si) frame (left) and gold-coated Si extractor grid (right).

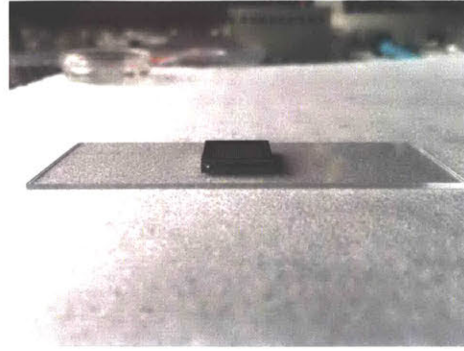

Figure 1-9: The assembled thruster package. At this point the thruster could be filled with ionic liquid and fired.

bulk. A CAD model of this packaging is shown in Figure 1-10.

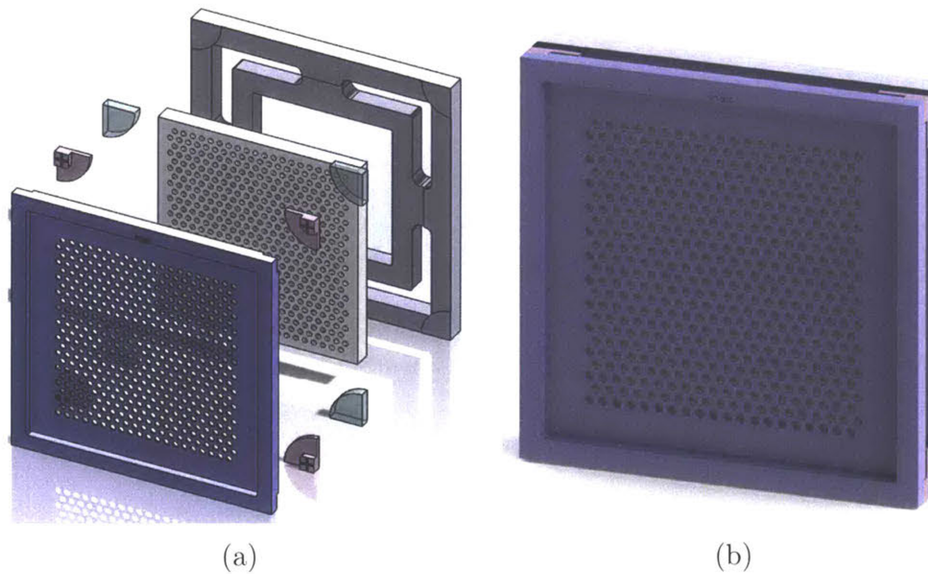

(a) (b)

Figure 1-10: CAD drawings of present iEPS packaging as designed by Louis Perna [10].

The iEPS package consists of three layers comprising a lower "frame," a porous substrate into which an array of emitters is etched by selectively removing material via laser ablation, and a grid of holes etched into a Si substrate using MEMS processing which is referred to as an extractor. Each of these layers is shown in Figure 1-10a. The three layers comprising the frame are a 13 mm x 13 mm x 1 mm base layer made of Si, a borosilicate glass insulating layer in each of the four corners of the base

layer, and a Si alignment layer on top of the quartz glass layer, which serves as a visual alignment for laser ablation and physical mount and alignment constraint for the extractor grid. The final alignment of extractor grid holes to array tips is done by eye through an optical microscope. The porous chip is attached to the Si frame using a hardened adhesive.

Because the emitters need to be aligned to the holes of the extractor grid, it is important that the emitters and holes are co-located to within a few tens of microns relative to the corner alignment posts. To achieve this, the porous chip is attached to the frame first and then the emitters are laser ablated. This allows the chips to be attached to the frame with a less stringent requirement on placement, making assembly easier. Once laser ablation has occurred, the extractors are held in place either using low-outgassing Teflon screws or, if permanent attachment is necessary, using a room-temperature epoxy.

The ionic liquid propellant is fed to the emitters through the back of the chip through a square port in the base layer of the frame, visible in Figure 1-10a. The propellant is passively drawn to the emitters through capillary action, which reduces the complexity of iEPS by not requiring a pressurized propellant feed system. If long-duration tests are not required, a small amount of propellant introduced to the chip from the back suffices to test the thruster's characteristics and performance in a vacuum chamber. For longer tests, a polyether ether ketone (PEEK) plastic propellant tank has been developed by the SPL to provide enough propellant for hundreds of hours of firing while simultaneously allowing for gasses and liquids trapped in the ionic liquid such as air and water from the atmosphere to outgas and leave the propellant tank without over-pressurizing it and causing the liquid to overflow from the chip. As we will see, ionic liquid containment is one of the main challenges to successfully implementing iEPS.

The voltage is applied directly to the ionic liquid by way of a carbon xerogel electrode upstream of the emitter array and the extractor grid is tied to spacecraft

ground, completing the circuit. The carbon xerogel electrode was developed primarily by Steven Arestie as part of his Master's thesis work in response to the occurrence of electrochemistry during thruster operation [11]. Early designs of iEPS utilized a porous nickel emitter which conveniently – or so it was thought at the time – doubled as a high voltage electrode. However, thrusters were failing after seconds or minutes and it was determined that this was due to electrochemistry at the interface between the electrode and the liquid, causing electrochemical breakdown of the ionic liquid as well as degradation of the emitter array tips [12]. The work done in [12] showed the feasibility of using a distal electrode to eliminate this electrochemistry, and the carbon aerogel electrode developed by Arestie showed tremendous resistance to electrochemical breakdown, in part due to its extremely high surface-area-to-volume ratio.

The voltage applied to induce ion emission is alternated to prevent charge accumulation within a single thruster. Since thrusters can only emit one species of ion at a time, thrusters must be operated in pairs at opposite voltages to ensure the spacecraft doesn't become charged in one polarity or the other.

1.3 Present State of the Art and Main Challenges

A critical feature of Taylor cone emission is its non-linearity. Emission from a Taylor cone will not begin until a critical electric field strength has been achieved, but current emitted from a single Taylor cone will also not increase indefinitely with increasing field strength [13],[14]. This means that in order to increase overall emission from an iEPS thruster, the number of emitters must be increased. iEPS as tested and manufactured by the SPL consists of an array of 480 emitters in a hexagonal array with the sites spaced 450 μm apart (this distance is referred to as pitch). The thrust produced by a single iEPS thruster is about 12 μN in an area of 1.69 cm^2, giving a thrust density of about 0.07 N/m^2 [15]. This is 1-2 orders of magnitude lower than

ion and Hall thrusters, which tend to have thrust densities of 1-2 N/m^2. Increasing thrust density of iEPS means increasing the area density of emitters, which in turn means placing emitters closer together. Tip density via laser ablation is limited by the beam spot size of the laser, which is limited in accuracy to tens of µm, and therefore sets a lower limit on how close emitters can be placed together. This naturally raises the question of whether there exists an alternative manufacturing method which could potentially allow for higher-density arrays, and therefore correspondingly higher thrust densities. The SPL's experience with MEMS pointed to leveraging the nano-scale precision offered by MEMS processes to create high-density, extremely precise arrays of emitters. iEPS thrust density scales linearly with the number of emitters, but the number of sites scales with the inverse square of pitch; therefore, decreasing pitch from 450 µm to 150 µm increases thrust density by almost an order of magnitude, and decreasing pitch further to 100 µm puts iEPS thrust density squarely in the range of ion and Hall thrusters.

The first part of this work examines the design and fabrication of Si molds for additive manufacturing of iEPS arrays. Additive manufacturing refers to adding substrate material to a mold, which is then selectively removed leaving only the substrate remaining. This work fully implements the idea first explored by Julie Xie in her Master's thesis, which showed the potential for forming emitters by sintering glass beads in a Si mold and then etching away the Si, leaving only the porous substrate remaining [16].

Because the ionic liquid propellant is conductive, leaks of propellant onto the surrounding electronics of the satellite can easily be fatal to both thruster and spacecraft operation, meaning containment is of utmost importance. Cessation of thruster tests during vacuum chamber testing tend to be for one of two reasons: either the propellant in the tank is exhausted, or the extractor grid is shorted to the propellant due to unintended electrical contact. In case of short circuits, these shorts develop in a variety of ways: when liquid is pulled above the top surface of the emitter chip and eventually makes contact with the extractor grid in an effect known as "flooding" or

"pooling," when discharges occur between the extractor grid and emitters, leaving a solid carbonized buildup that grows during thruster operation until making permanent contact with the extractor grid, and when liquid escapes from the portion of the thruster in contact with the Si frame and "creeps" to the posts, eventually bridging the insulating glass layer. Larger-than-ideal pores contribute to this by exerting a lower capillary force on the liquid and making it easier for containment to be lost. Surface coatings have been used to increase hydrophobicity on the surface of the emitters, but implementing uniform, nanometer-thin coatings on a highly non-uniform surface while preserving the hydrophilicity of the internal pore network is a daunting task. What's more, these coatings are limited in their effectiveness by non-uniform pore sizes and can still fail to contain the propellant if the pore size varies too much. If these coatings can be obviated by smaller, more uniform pore sizes, this means significant savings of cost and manufacturing complexity.

Additionally, material non-uniformity contributes to anomalous feature formation during laser ablation. The borosilicate glass chips used by the SPL for the first iEPS space missions are 1 mm x 1 mm square filter discs made by ROBU Glasfilter-Geraete GmbH. These chips often have small pieces of non-borosilicate glass interspersed throughout, which have different ablation rates during the laser ablation process and leads to the aforementioned anomalous features. These typically manifest as emitters in locations where none should be and are evidence that emitter substrate uniformity can have a material impact on thruster quality and performance.

Chapter 2

Array Molding and Fabrication

The potential to utilize MEMS processing technology for emitter array fabrication was demonstrated by Xie in her Master's thesis. Her work showed that it could be feasible to create porous substrates inside of a Si mold and then etch away the mold, leaving the porous substrates behind. The reason for using MEMS to create these molds is due to its extremely high precision; repeatable structures on the nanometer scale are achievable using established processes including photomasking and reactive-ion etching (RIE). One of the main challenges for iEPS is increasing the thrust density, which requires decreasing the separation between individual emitters in an emitter array. Precisely controlling the amount of material removed by laser ablation becomes extremely difficult at scales below tens of microns, and indicates a different manufacturing method might need to be pursued in order to achieve this densification.

2.1 Mold Design and Fabrication

Si molds were produced using batch MEMS processing on 6" diameter, 650 µm thick silicon-on-insulator (SOI) wafers. The wafers had a 500 µm handle side, 1 µm buried

oxide (BOx) layer, and 150 µm device layer. Each wafer contained 109 individual molds or "dies," with an array of channels which varied in diameter and pitch. Dies were designed with three different pitches: 100 µm, 225 µm, and 450 µm. The 450 µm pitch, despite being the same as presently used in iEPS state of the art, was chosen due to its compatibility with existing extractor designs and would allow for rapid testing once tip structures were achieved. The MEMS processing steps, based on Xie's work, are illustrated in Figure 2-1 [16].

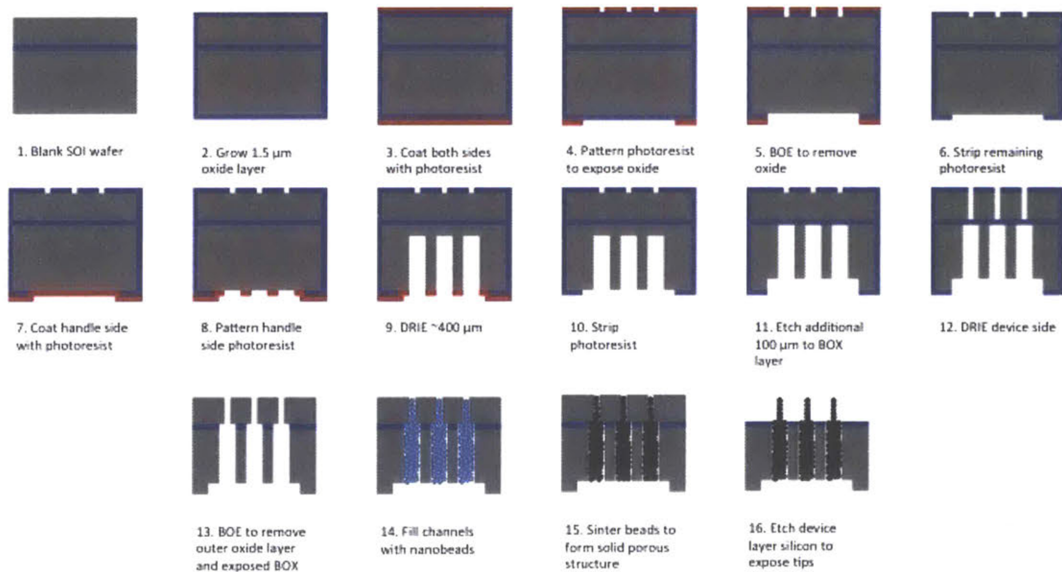

Figure 2-1: The MEMS processing steps for creating the Si molds, including addition and sintering of material to create the porous emitters and network. Steps are also laid out in Table 2.2.

The process was designed such that cylinders etched into the top of the dies had a smaller diameter than the cylinders etched into the bottom of the dies. This was to allow the dies to be filled from the back with a mixture of beads and liquid, and the capillary force would increase with the decreasing cylinder diameter. This would help pull the bead mixture into the cylinders and facilitate complete filling of the mold, ensuring a more even porous substrate.

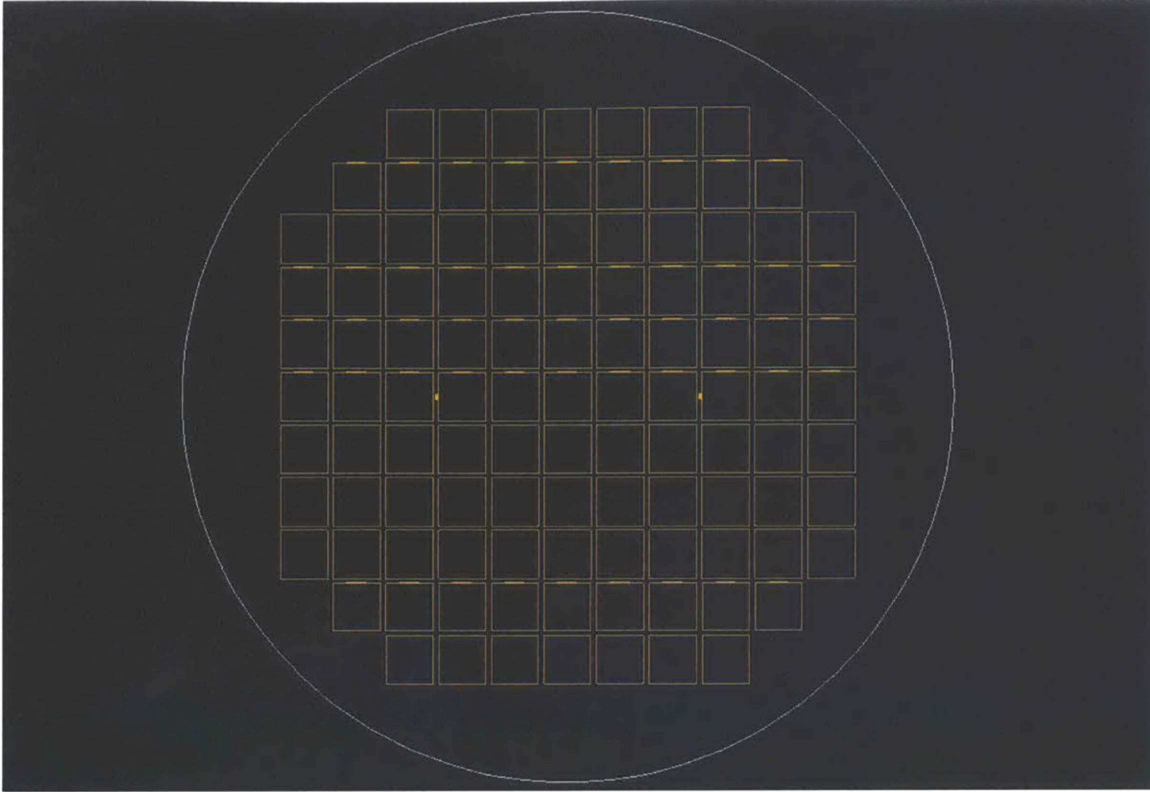

Figure 2-2: Wafer with outlines of individual mold dies. Each wafer contains 109 dies.

The column diameters, pitches, and number of each type of mold are laid out in Table 2.1:

Pitch (µm)	Total # of Dies	D_{Device} (µm)	D_{Handle} (µm)
100	8	24-36	50
225	77	24-48	100
450	24	24-64	200

Table 2.1: Number of dies, range of diameters for top side columns (in 2 µm increments for the 100 pitch dies, 4 µm increments for the 225 µm and 450 µm pitch dies), and back side column diameters.

The molds were fabricated in the MIT Microsystems Technology Laboratory (MTL) using standard MEMS processing techniques:

Step	Process
1	RCA Clean of SOI wafer
2	3-4 μm oxide deposition on 500 µm handle side
3	Coat and pattern handle side oxide layer to create nested mask
4	Coat and pattern handle side photoresist
5	Etch handle side 250-400 µm
6	Strip photoresist
7	Continue etch to BOx
8	Mount to handle wafer
9	Coat and pattern device side photoresist
10	Etch device side to BOx
11	Dismount handle wafer
12	BOE to remove all oxides
13	O_2 Ashing, piranha to remove residual fluoropolymer and photoresist
14	Dice finished wafer on die saw

Table 2.2: Table of steps in the mold fabrication process.

2.2 Materials Testing

Materials tested in the molds included soda-lime glass and silicon dioxide (SiO_2) micro-beads, and titania and resorcinol-formaldehyde xerogels. The materials were introduced to the molds in different ways depending on their functional form: the xerogels were liquid and so were introduced to the molds from the back, while the soda-lime glass was initially introduced by making a mixture of the powder with water or isopropyl alcohol. However, it was soon discovered that pressing the dry powder into the molds with a gloved finger provided a much more effective and consistent method of introducing the beads to the molds. These beads were then sintered to form a permanent porous structure.

2.2.1 Sintering

Sintering is a method of creating a solid structure from a loose powder by heating a material to its glass transition temperature and causing the outer portion of the powdered beads to flow together with adjacent beads. The sintering process is illustrated

in Figure 2-3:

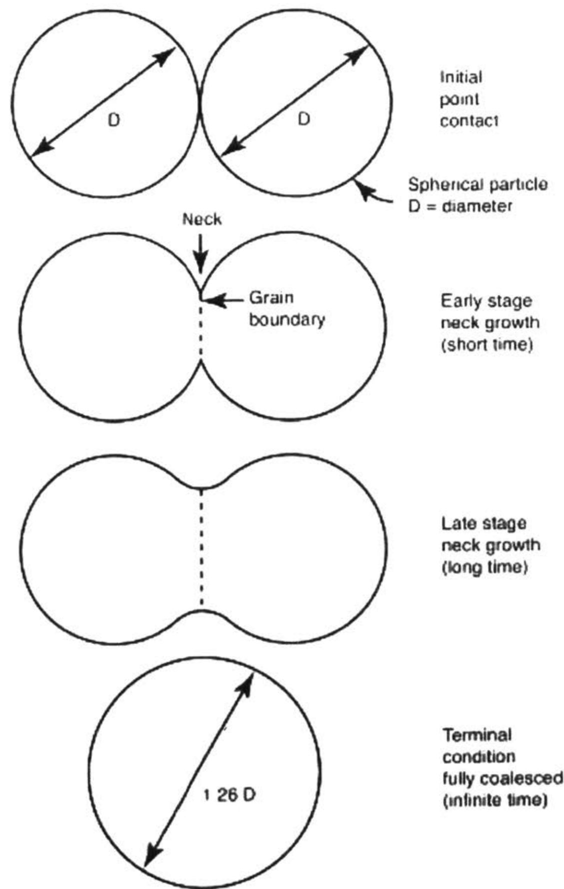

Figure 2-3: A diagram of the sintering process [4].

A key component of sintering is that it doesn't require the material to be heated to its melting temperature to be sintered, making temperature requirements less stringent. Sintering temperature also falls as particle diameter decreases, which can lessen the requirements on equipment and material selection.

2.2.2 Soda-Lime Glass Beads

The same soda-lime glass beads utilized by Xie were used for this work. These beads were obtained from Cospheric LLC and were polydisperse in size, with a median bead

diameter of roughly 4 µm, a D10 of less than 2 µm, and a D90 of less than 6 µm. This polydispersity was a drawback for the sintering process because it meant smaller beads would be completely melted, while larger beads would not be sintered at all. Figure 2-4 shows a scanning electron microscopy (SEM) image of the beads after sintering as well as the differences in bead sizes.

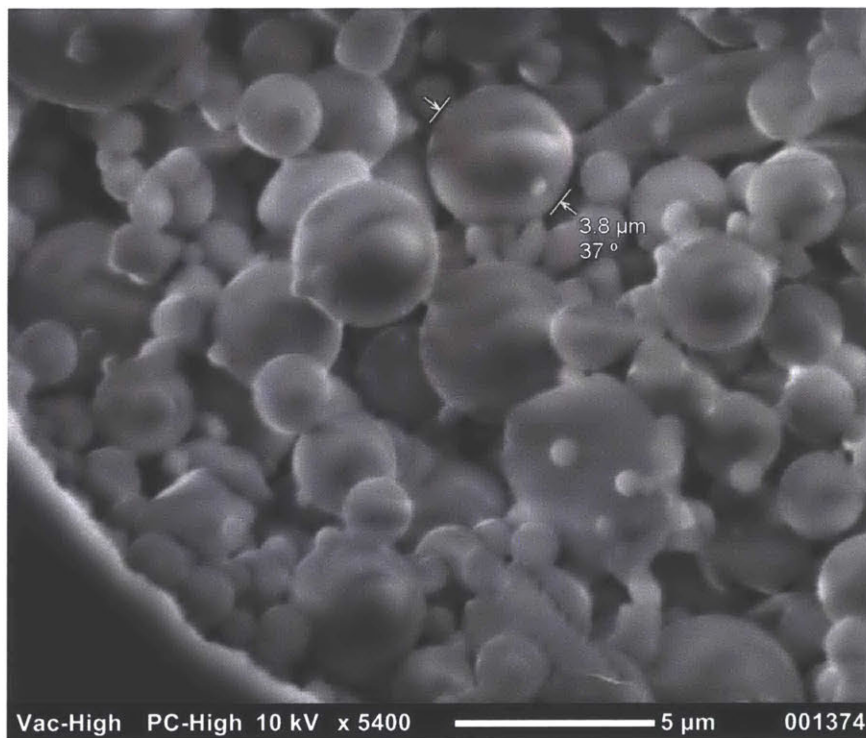

Figure 2-4: SEM image of soda-lime glass beads after sintering. Note the wide range of bead sizes as well as the variability in sintering.

The beads were sintered at 595 °C for two hours to ensure equilibration of temperature throughout the sample. The temperature was raised and lowered at a rate of +3 °C/min and -4 °C/min respectively. This is shown in Figure 2-5.

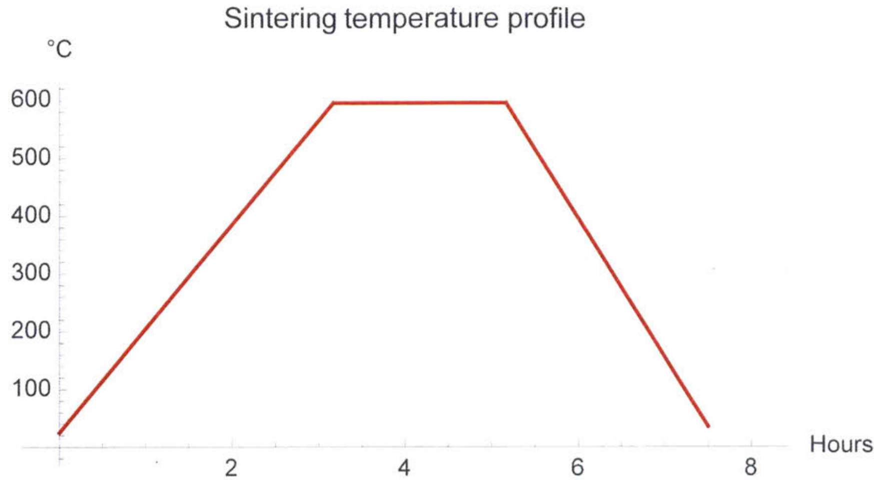

Figure 2-5: Sintering profile vs. time in hours: +3 C/min rise, 2 hour hold at 595 °C, -4 C/min cooling rate.

Pore sizes in substrates created with the soda-lime glass beads tend to be on the order of 1-5 µm. As mentioned, polydispersity of bead sizes was an important drawback, and at the larger end, the beads were 12-15 µm in diameter. For some of the mold channels, this was more than half the diameter of the channel, meaning that just two of them could completely block a channel. However, the ease with which the molds could be filled using the dry powder as well as the beads' resistance to etching in the MTL RIE machines made it the best-performing material tested in these experiments.

Experiments demonstrated that variation in particle diameter played a central role in quality of finished arrays. Completeness of sintering varied widely as a function of diameter with the largest beads (10-15 µm) remaining unsintered while the smallest beads (0.5-3 µm) were often completely melted. 5 µm filters were purchased and mounted on the end of a syringe filled with a DI water-soda-lime micro-bead mixture with the intent of pushing the slurry through the filter. However, in all tests the plastic housing which contained the filter simply deformed under pressure and allowed the mixture a path around the filter instead of through it. Addressing this issue could lead to greatly improved emitters and array characteristics.

2.2.3 Xerogels

Xerogels are a type of porous material which have been tested in the SPL due to their highly controllable pore size and porosity [17],[18],[11]. These materials also have an extremely high surface area to volume ratio, and are of the same class of materials used to make distal electrodes in iEPS fuel tanks. Resorcinol-formaldehyde (RF) and titania (TiO_2) xerogels were tested as part of this work. The xerogels were made with the following recipes as developed by Jimmy A. Rojas-Herrera in the SPL:

Step	Process
1	Mix 2.46 g of resorcinol with 3 g of deionized water
2	Stir
3	Add 4.3 g of formaldehyde 37%
4	Add 0.088 g of acetic acid
5	Place in sealed container for 18 hours
6	Place in furnace at 40 °C for 6 hours
7	Place in furnace at 60 °C for 18 hours
8	Place in furnace at 80 °C for 30 hours

Table 2.3: Steps to make RF xerogel.

Step	Process
1	Mix 4.80 g of deionized water with 8.90 g of HCl 2M
2	Add 0.7 g of formamide
3	Mix 1.00 ml of TiO_2 with 2.73 ml of isopropyl alcohol
4	Add TiO_2-IPA mixture to water-HCl-formamide solution
5	Place in furnace at 60 °C for 24 hours
6	Place in furnace at 80 °C for 72 hours

Table 2.4: Steps to make titania xerogel.

However, xerogels have a number of drawbacks which preclude successful use in this manufacturing method. The first is the formation of a non-porous skin on the outer layer of RF as shown in Figure 2-6. These are not a problem when making bulk porous xerogels since the non-porous skin can be removed by "sanding," however, this option was not available in molds.

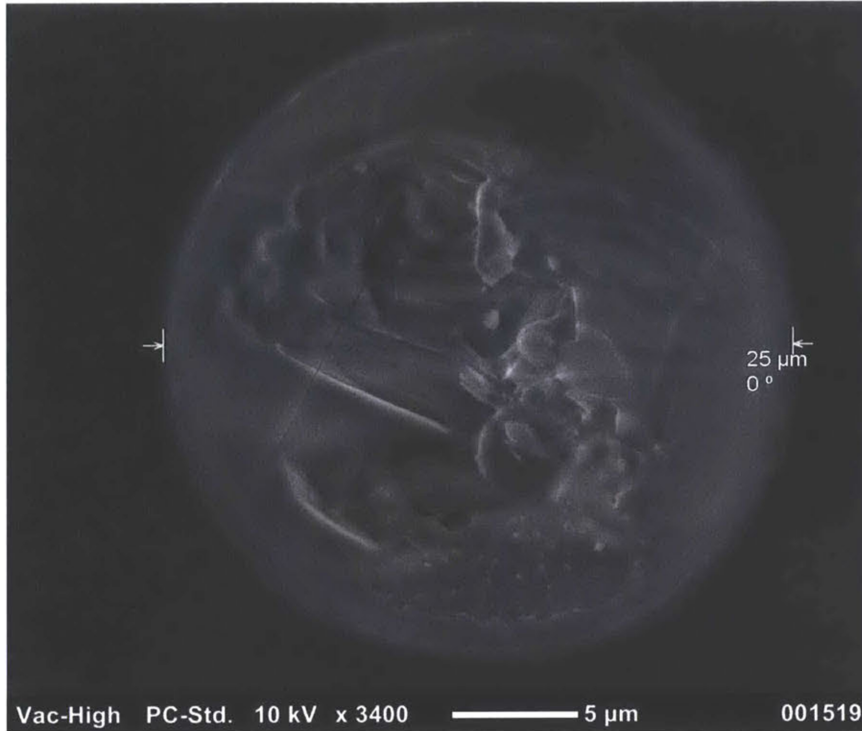

Figure 2-6: Non-porous skin on outer surface of RF substrate material.

The second drawback was the xerogel's lack of resistance to both wet and dry etches. The material simply etches away in a sulfur hexafluoride (SF_6) plasma (Figure 2-7) or a TMAH wet etch bath (Figure 2-8), leaving no tip array regardless of the presence of the non-porous skin.

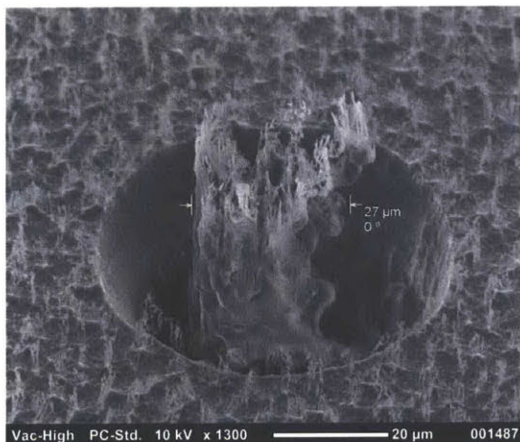

Figure 2-7: RF etched by RIE plasma.

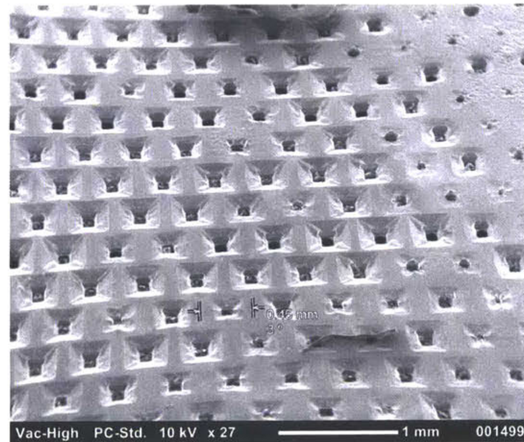

Figure 2-8: RF after etching in TMAH. No RF remains.

Attempts were made to synthesize titania xerogels, however none successfully dried to a solid phase, and therefore failed to create a porous array.

2.2.4 Silicon Dioxide (SiO_2) Micro-Spheres

SiO_2 micro-spheres were examined due to their extremely uniform size distribution and highly controllable diameter. Unlike their soda-lime glass counterparts, SiO_2 micro-spheres have no noticeable variation in diameter, which potentially allows for highly controllable tip size and shape depending on mold parameters. Micro-spheres of 2 µm diameter were obtained from Cospheric LLC. As with aerogels, however, several drawbacks exist which prevented their implementation in our arrays.

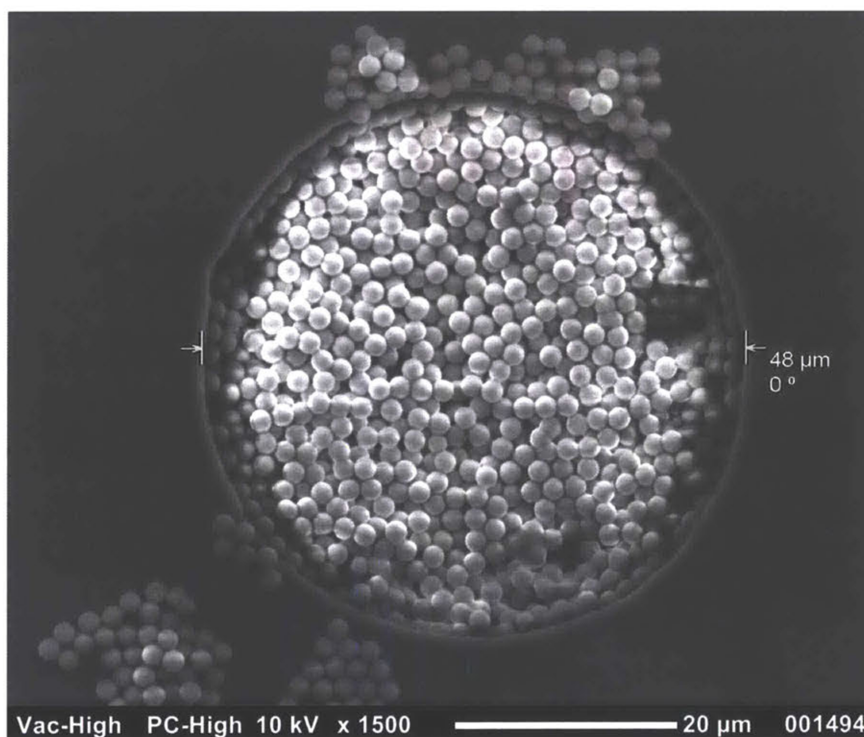

Figure 2-9: 2 µm SiO_2 microbeads in a mold channel. The high degree of uniformity is apparent from this SEM.

Unlike soda-lime glass micro-spheres which have a sintering temperature of around 595 °C and can therefore be sintered in a tabletop furnace, 2 µm SiO_2 beads have a

sintering temperature higher than the 1100 °C maximum temperature of the SPL's tabletop furnace, a Thermo Scientific Lindberg Blue M, which meant that method of joining beads together to make a solid array was unavailable. Also similar to xerogels was the characteristic that the SiO_2 micro-spheres etched at roughly the same rate as the Si molds in the available etching machine, leaving no array. While researching materials we discovered soda-lime nano-spheres of ~24 nm diameter and it was hoped the small size would allow them to be effectively re-flowed at relatively low temperature (300 °C) and provide both etch-proof coating for the SiO_2 as well as a binding agent to effectively provide the same effect as if the outer surface had been sintered.

To implement the nano-sphere coating, the dilution of soda-lime nano-spheres in DI water was adjusted such that the volume of nano-spheres in the liquid would roughly equal the volume needed to ensure a complete coating of the micro-spheres. This was found to be 12.5%, although nano-sphere concentrations of 25% and 50% by weight were also tested.

Figure 2-10: SiO_2 micro-spheres coated and bound using soda-lime nano-spheres. If SiO_2 was not fully covered by soda-lime, it was etched away.

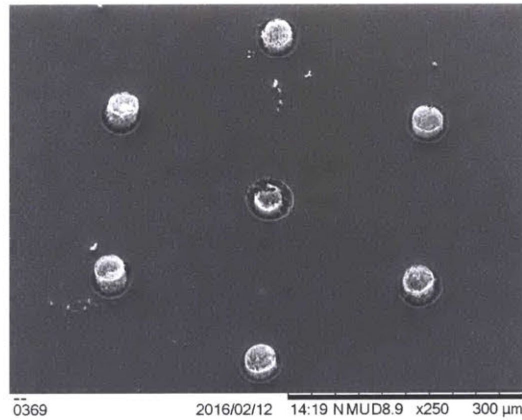

Figure 2-11: A cluster of partially-etched emitters. Most channels were unfilled or partially filled.

As is shown in Figure 2-10, the soda-lime nano-spheres did not provide a consistent coating. SiO_2 micro-spheres near the "top" side of the column during the drying

process were often uncoated or partially coated while "lower" down the column the spaces between the micro-spheres were often completely filled, leaving no porosity. It was found that varying the concentration of nano-spheres did not improve the consistency of the coating.

2.3 Production of Arrays

Arrays of finished emitters were successfully created using soda-lime glass micro-spheres sintered at 595 °C. The filled molds were then taken to a Plasmatherm RIE machine located in the Exploratory Materials Lab (EML), a facility located within the MIT MTL. The molds were etched for 9-11 hours in a 30 standard cm^3/min (sccm) SF_6 + 3 sccm oxygen (O_2) plasma at 200 W and 40 mTorr. The etch is fairly isotropic, although the $Si:SiO_2$ selectivity of the machine is a very poor 2:1. Figures 2-12 and 2-17 show a single etched emitter and 450 µm array of emitters respectively after etching in the EML.

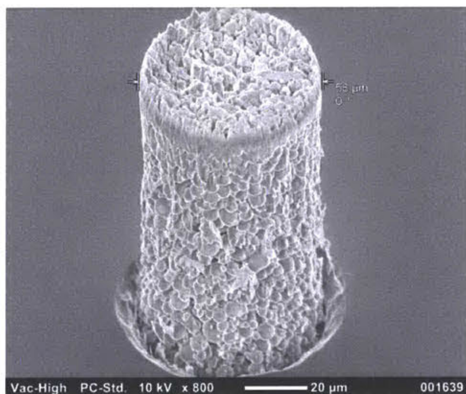

Figure 2-12: A single 57 µm diameter soda-lime glass emitter after mold etching.

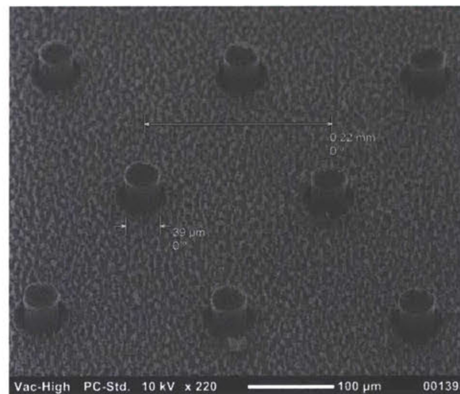

Figure 2-13: A 225 µm pitch array with 38 µm channels after approximately 50 µm of etching.

An interesting phenomenon was observed while etching these molds. In Figures 2-7, 2-11, 2-14, 2-15, and 2-17, white grass-like structures can be seen on the Si around the emitters. This was caused by etching and re-deposition of a clear soda-lime glass microscope slide on which the samples were resting in the RIE machine. Placing the

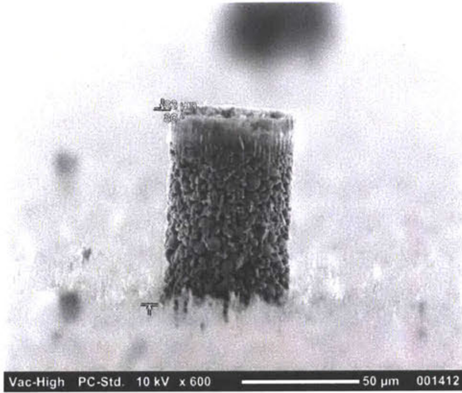

Figure 2-14: A 48 µm diameter column after 83 µm of etching.

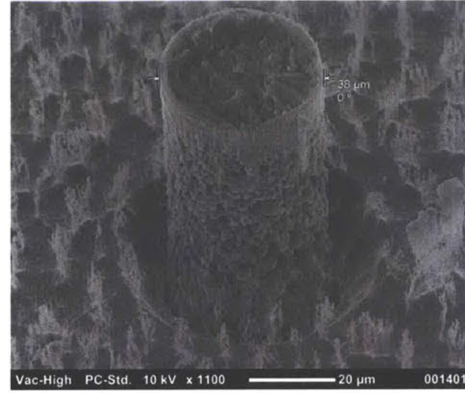

Figure 2-15: A single 38 µm column. Note the re-deposited glass from the microscope slide on which the die was resting.

molds directly on a Si carrier wafer eliminated this phenomenon.

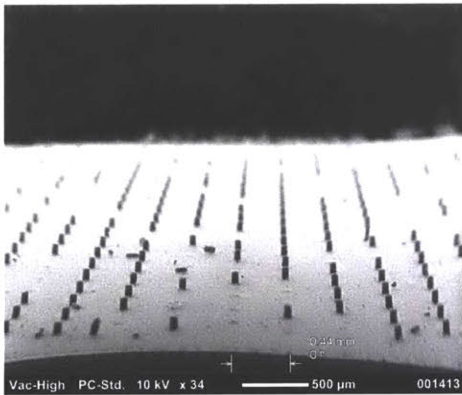

Figure 2-16: Side view of an array after part of the etching process. Some columns were knocked over during handling.

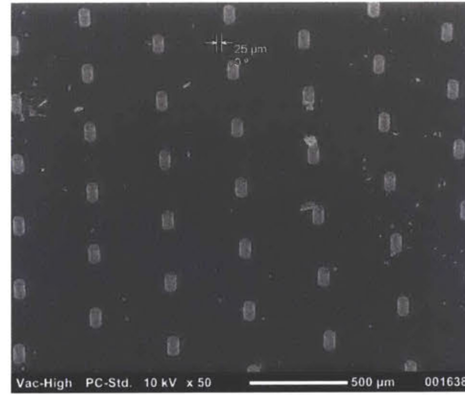

Figure 2-17: Array of 450 µm pitch, 57 μm diameter soda-lime glass emitters after mold etching.

To test finished arrays, the Si die was bonded to an existing Si frame package used for traditional iEPS thrusters and aligned to an extractor by eye. The Si was secured to the frame using a room temperature epoxy and filled with 1-Ethyl-3-Methylimidazolium Tetrafluoroborate (EMI-BF_4) ionic liquid from the handle side, showing thorough hydrophilicity (visible as a uniform darkening of the tops of the emitters) as seen in Figure 2-18. Of note is the lack of spreading of the ionic liquid across the Si. The slight pitting around the emitters, most clearly visible in Figure

2-15, is caused by ion deflection at the base of the emitters and results in pooling at the base; however, ionic liquid containment was not an issue prior to starting the test. Because this thruster was not mounted to a tank, it was only fired for a few minutes (see section 4.1) and it is unclear if the type of pooling that becomes an issue with extended firing of borosilicate glass emitter chips is also an issue with molded Si arrays.

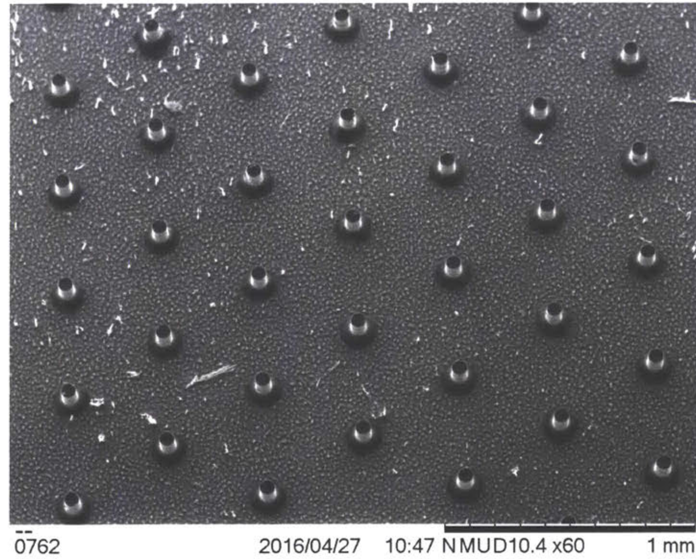

Figure 2-18: 450 μm pitch array filled with EMI-BF_4 ionic liquid. Darker spots indicate a conductive substance, in this case the EMI-BF_4.

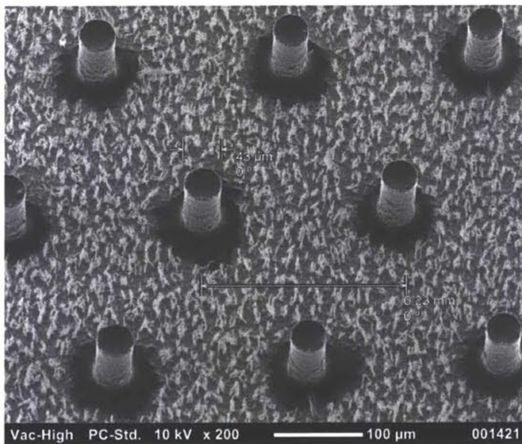

Figure 2-19: A 225 µm array of 43 µm cylinders filled with ionic liquid.

Figure 2-20: A single 43 µm tip from a 225 µm pitch array filled with ionic liquid.

Chapter 3

SiO_2 Array Fabrication

3.1 Current Methods and Challenges

Production emitter arrays are manufactured as part of a multi-step process which involves the fabrication of a Si packaging frame with glass corner posts for insulation, bonding a blank emitter chip to the Si frame, and patterning the chip using laser ablation to selectively remove material and form the emitter tips. The porous substrates are 1 cm x 1 cm sintered borosilicate glass filters with a pore size of approximately 1-5 µm and a porosity of approximately 40%. The chips are filed to a thickness of just under 1000 µm to ensure the tips are flush with the bottom plane of the extractor grids to minimize required emission voltage. An SEM of a borosilicate chip is shown in Figure 3-1.

Figure 3-1: SEM of a borosilicate chip used to fabricate emitters. Note the irregularity in particle size and the resulting surface roughness and pore size variation.

Of note is the degree of variation in pore size and shape due to the range of particles used to make the chips. This is a drawback for a number of reasons. It means that the pore sizes at the very tip of the emitters will vary across an array, which means uneven emission characteristics for a thruster. It also means that some of the pores will exert a lower capillary force on the ionic liquid, possibly leading to a lack of containment and subsequent pooling or flooding of the emitter arrays and, ultimately, a failure of the thruster. This phenomenon is shown in Figure 3-2.

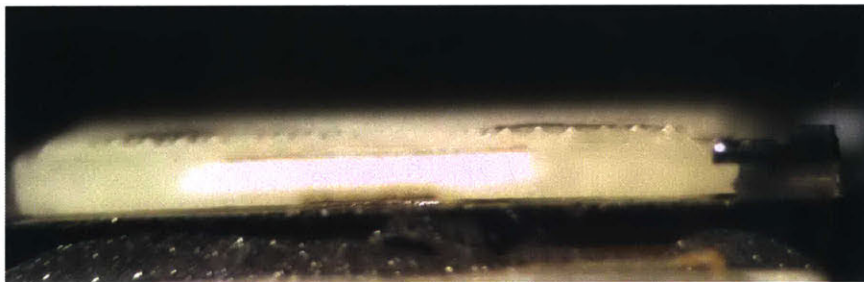

Figure 3-2: Pools of ionic liquid visible on the right and left side of the emitter array surface. This type of pooling will short circuit the thruster and prevent it from operating.

Another type of thruster failure related to ionic liquid containment is what is known as creep. This is when ionic liquid escapes the containment of the chip at the interface between the chip and the material bonding the chip to the frame. The liquid moves along the Si frame and creeps across the glass insulating layer in the posts, resulting in electrical contact between the ionic liquid and extractor grid, shorting the thruster.

This has a significant negative impact on thruster lifetime. Electric propulsion systems, due to their low thrust, need to be able to fire for much longer durations than their chemical counterparts, and for many missions this means thousands or tens of thousands of hours of firing. If a thruster fails due to ionic liquid containment issues, this typically happens on the order of 50-100 hours, and eliminating this drawback has the potential to significantly increase the lifetime and mission capability of these thrusters.

(a)

(b)

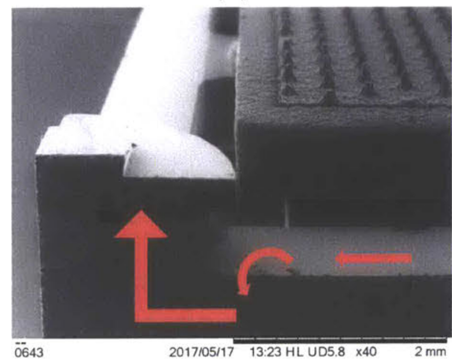

(c)

Figure 3-3: SEMs of a borosilicate emitter chip illustrating the creep phenomenon: (a) Ionic liquid escapes at the interface between chip and bond. (b) Ionic liquid creeps along Si frame due to electrical stresses. (c) Ionic liquid creeps from frame to corner post, eventually bridging the glass insulating layer of the posts.

Various surface coatings have been tested with the aim of increasing the hydrophobicity of the surface of the borosilicate emitter glass after the laser ablation step using chemical vapor deposition (CVD) and physical vapor deposition (PVD) processes. One of the principal challenges of implementing surface

coatings is evenly coating a highly-irregular
surface like those of iEPS emitters. In the case of PVD, if the deposition angle is within 10-25°of the axis normal to the plane of the emitter chip, the tip of the emitters tend to accumulate the most coating, while the trenches between emitters accumulate the least. This is exactly the opposite of the ideal scenario; the purpose of the hydrophobic coating is to minimize the ability of the ionic liquid to escape from the bulk of the emitter chip, while still preserving a relatively low impedance in the tips themselves as well as minimize the required operational voltage for the thruster. An accumulation of coating on the tips also changes the tip geometry, which can not only lead to higher or unattainable operational voltages, but can also change the firing angle of the Taylor cone such that it doesn't fire through the extractor grid, but rather into it. Difficulties with frequent machine reservations and contamination made it challenging to reliably implement coatings and highlight the importance of pursuing a more uniform emitter material.

An examination of the laws of capillary action can provide some insight into why creating a substrate made from uniform spherical particles could be effective in addressing the liquid containment issue. The Young-Laplace equation gives the pressure drop across a liquid interface as a function of the surface tension, γ, and principal radii of curvature, R_1 and R_2:

$$\Delta p = \gamma \left(\frac{1}{R_1} + \frac{1}{R_2} \right) \tag{3.1}$$

In the context of an iEPS thruster operating in space, the external pressure is zero, and we will assume for the sake of argument that the spheres are perfectly wetting; in other words, the propellant will have zero contact angle with the spheres and the capillary force will be maximized. The condition of flooding in the context of Figure 3-4 corresponds to the surface of the liquid being pushed above the highest point on the spheres by internal pressure. For a sphere, $R_1 = R_2 = R$, and we assume the beads are evenly packed, so the radius of curvature in the plane orthogonal to the

diagram is also R.

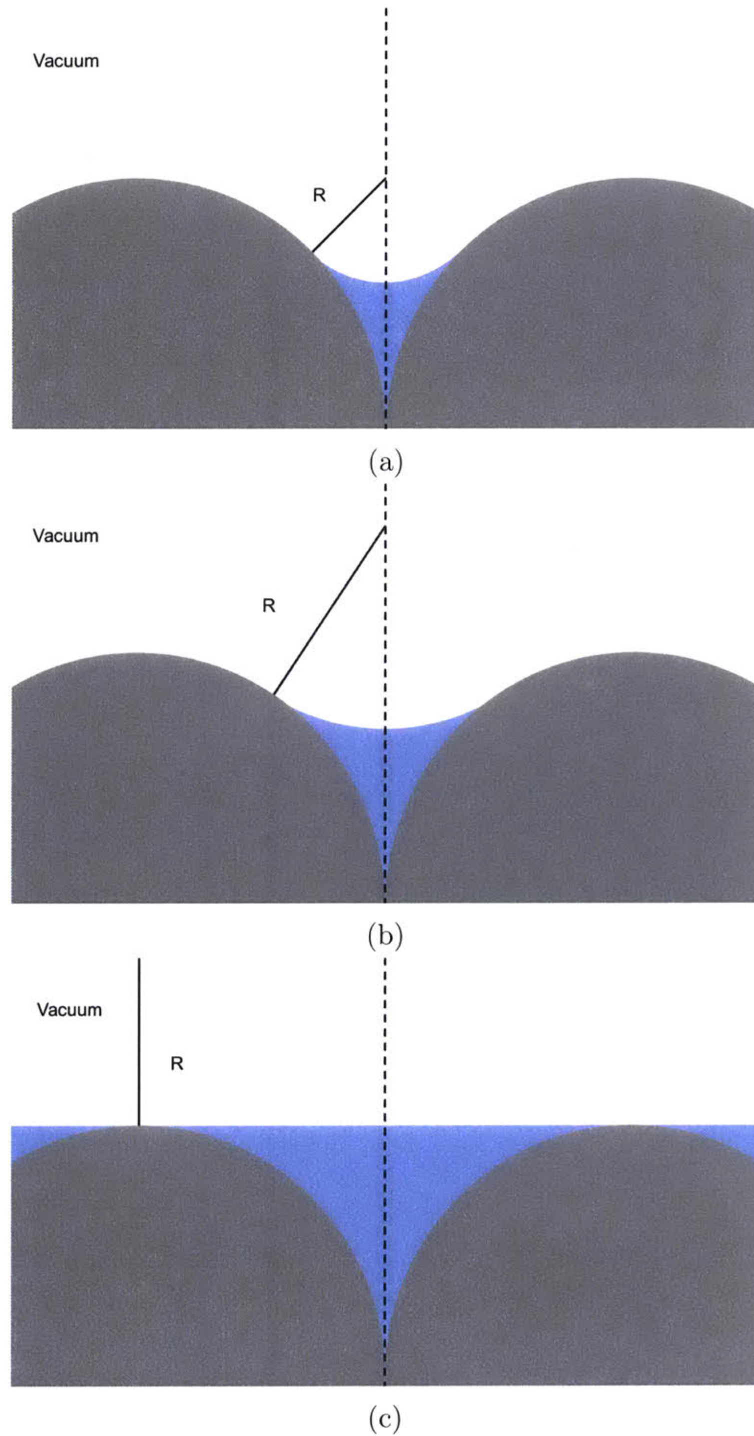

Figure 3-4: Diagram of the wetting process illustrating increasing radii of curvature in the Young-Laplace equation, causing the pressure difference between liquid and vacuum to go to zero as liquid height increases in a uniform layer of spheres.

As the liquid is pushed higher up the face of the sphere, the principal radii of curvature increase, causing the pressure to fall. When the surface of the liquid becomes tangent to the top of the sphere, R_1 and R_2 are parallel to one another, and equation 3.1 goes to 0. Alternatively, in the condition where one or both of the principal radii of curvature is negative, the $\Delta p = 0$ condition is reached before the liquid reaches the surface of the beads. This means there is no longer pressure forcing the liquid upwards, preventing flooding. In reality, the beads will not be perfectly hydrophilic and the liquid should remain confined below the top of the beads.

3.2 Hydraulic Pressing of Emitter Chips

3.2.1 Method

In the ideal scenario, the physical properties of the emitter chip would obviate the need for additional coatings. Given the lessons learned from our efforts to mold emitter arrays as detailed in chapter 2, it became apparent that one of the main drawbacks of the soda-lime micro-beads was their variation in diameter. SiO_2 micro-beads tested as part of that work were roughly 2 μm in diameter and did not sinter in our tabletop furnace. After some searching, however, SiO_2 nano-beads of 750 nm diameter in powder form were procured from Fiber Optic Center, Inc. These beads were relatively cheap and available in 1 kg quantities. A variety of solvent mixtures, temperature profiles, and furnace gases were tested over the course of this research and a recipe for the repeatable production of these chips was achieved.

The first test of sintering was done in a box furnace at the Materials Research Furnaces, Inc. facility in Allenstown, NH. The powder was heated to 1250 °C in an alumina (Al_2O_3) crucible for 10 minutes. Though the powder showed some signs of sintering on both a macro scale (clumping together of the powder) and micro scale (see Figure 3-5), the green body failed to sinter into a unitary mass.

Figure 3-5: SEM of 750 nm SiO_2 beads sintered at 1250 °C. Lighter beads are closer to the electron detector and illustrate the lack of bead packing, which resulted in small chunks sintering together instead of a single sintered mass.

It was determined that the beads should be compacted before sintering to ensure better contact between neighboring beads and ensure a higher likelihood of creating a solid porous mass that could eventually be turned into an emitter chip. A hardened steel pressing die with a 13 mm x 13 mm cross section was purchased from Across International and is shown in Figure 3-6.

A hydraulic press located in the MIT Institute for Soldier Nanotechnologies (ISN) was used for initial tests; however, pressed greens were often damaged in transport from the ISN to the SPL and a 24-metric-ton hydraulic press was purchased from Across International, shown in Figure 3-7. The limiting factor was the pressing die, which was only capable of withstanding 15 metric tons before the center pressing column of steel permanently deformed at the edges, creating uneven stress in the greens and causing the chips to split into layers along the planar axis of the chip similar to what is shown in Figure 3-8.

Figure 3-6: 13 mm x 13 mm pressing die.

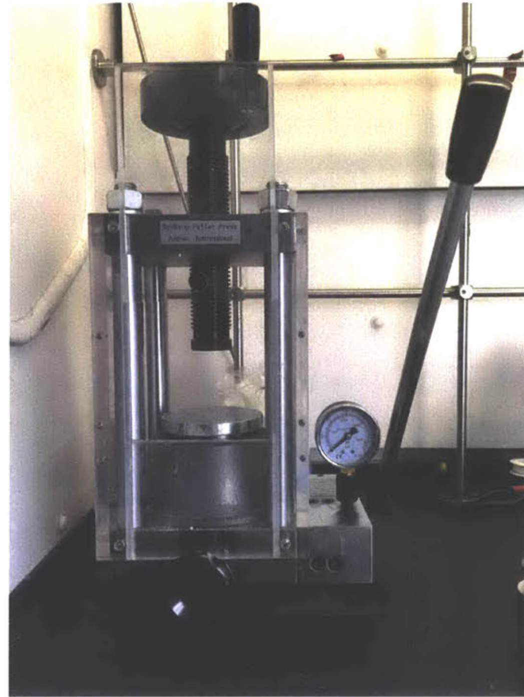

Figure 3-7: 24-ton hydraulic press.

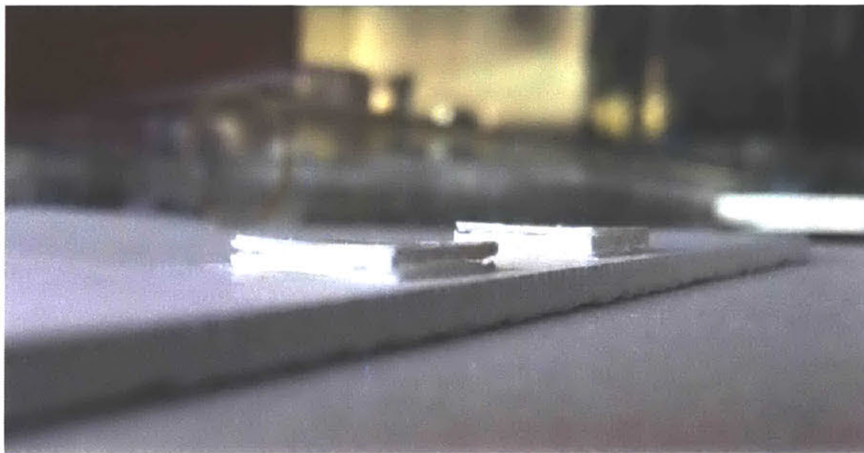

Figure 3-8: Planar layering in a chip after the sintering process at 1100 °C for 1 hour in a 5 sccm argon flow. This instance of layering was caused by heating the sample in the furnace before all of the water had time to evaporate, over-pressurizing the chip.

A mixture of SiO_2, deionized water, and lactic acid $<0.5\%$ by weight ($C_3H_6O_3$) was used to create a slurry, which produced the first sintered beads at 1100 °C for 1 hour in a 5 sccm flow of argon. The addition of lactic acid is to act as a dispersant to prevent the beads from clumping together unevenly and is based on the work of

Niu et al. [19]. An SEM of two different areas of the chip is shown in Figure 3-9 and shows that different areas of the chip underwent different levels of sintering.

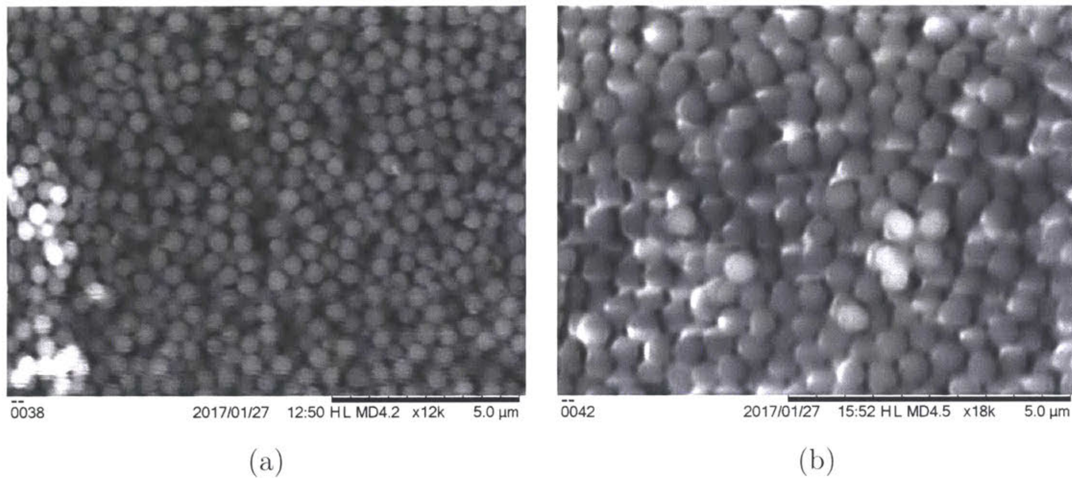

(a) (b)

Figure 3-9: Sintering of SiO_2 at 1100 °C. Differences in sintering are visible in different areas of the chip.

The uneven sintering has the effect of preventing the entire chip from forming a unitary porous mass, and has been one of the principal challenges preventing this method from replacing borosilicate glass as an emitter array material at the production scale. Figure 3-10 shows that simply picking up the chip and handling it is enough to cause the edges to break apart.

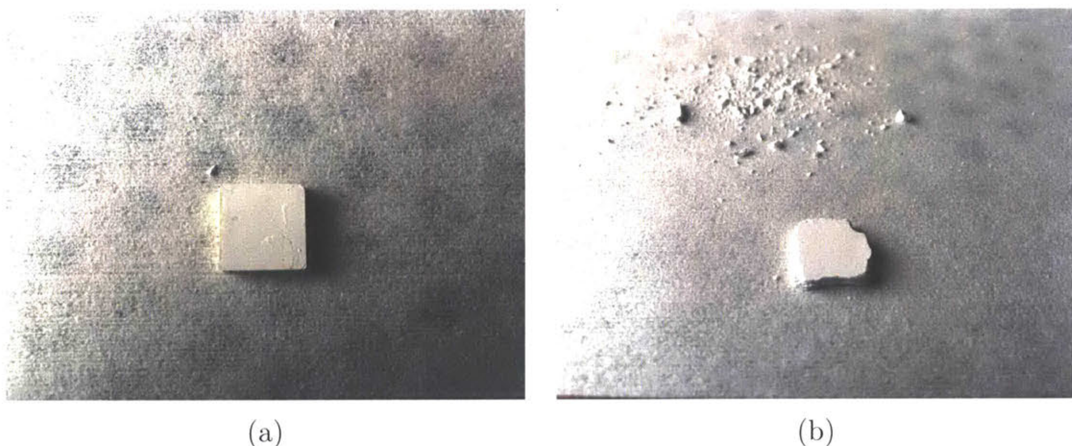

(a) (b)

Figure 3-10: A sintered chip before and after light handling.

Fortunately, because the emitter arrays are 10 mm x 10 mm and the molded greens are 13 mm x 13 mm, there is usually enough material left in order to make an emitter

chip. The principal recipe for creating chips was as follows:

Step	Process
1	Mix 99.5% DI water and 0.5% lactic acid by weight
2	Heat mixture at 80 °C to mix lactic acid
3	Add dry SiO_2 powder to mixture until mixture is difficult to stir
4	Fill die press with ~250 ml of mixture
5	Pressurize press to ~3600 psig or higher
6	Immediately release pressure
7	Gently de-mold green
8	Place in furnace and ramp temperature to 90 °C
9	Hold for one hour to let water evaporate
10	Start 5 sccm argon flow
11	Ramp temperature at +5-10 °C/min to 1100 °C, hold for 1-2 hours
12	Ramp temperature at -5-10 °C/min to room temperature

Table 3.1: Steps to make porous SiO_2 chips.

It was found that leaving the beads under pressure for longer than 20-30 seconds often resulted in the chips splitting apart along the planar axis as is shown in Figure 3-11.

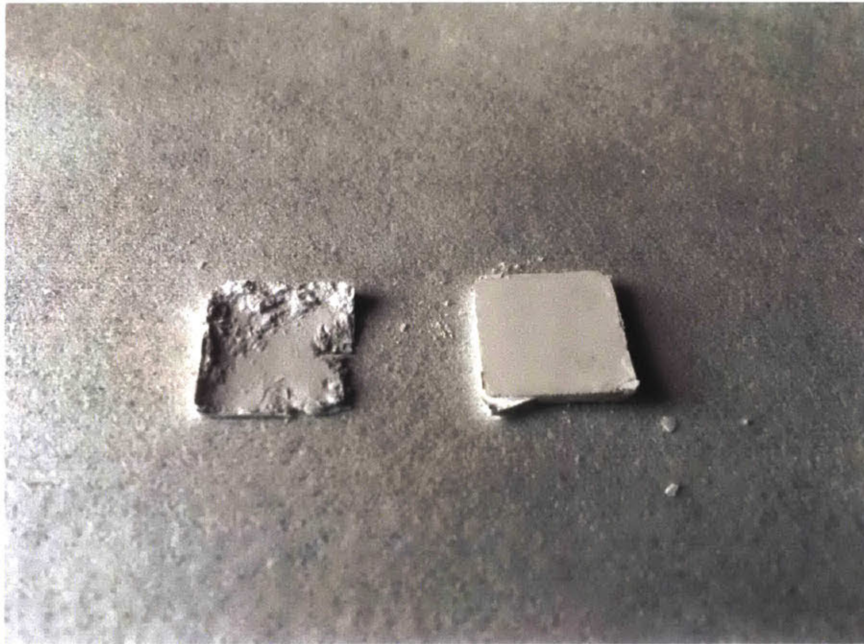

Figure 3-11: Planar layering in a chip after leaving the chip in the hydraulic press for 10 minutes. It was observed that layering occurred more frequently if the chips were left under pressure for durations greater than 20-30 seconds.

3.2.2 Alternate Mixtures and Furnace Recipes

A number of other process gasses and SiO_2 bead mixtures were tested as a means of achieving more reliably solid chips over which more control could be exerted in terms of filing to a specified shape and thickness. Alternate mixtures included the use of binders, different solvents, and more or less dispersant. The goal of using binders is to hold the beads close together during the sintering process, which should result in a more uniformly sintered chip. The following combinations were tried, with all producing sub-optimal results. Table 3.2 lists the combinations of mixtures and process gasses.

Solvent	Binder	Dispersant	Flow Gas	Result
DI Water	5-25 nm SiO_2 nanoparticles	Lactic Acid 0.5% wt.	5 sccm Ar	Non-porous chips
DI Water	Polyethylene Glycol 1% wt.	Lactic Acid 0.5% wt.	5 sccm Ar	Poor sintering
DI Water	None	Lactic Acid 0.5% wt.	5 sccm CO_2	Layering caused by increased sintering on external chip faces
DI Water	None	Lactic Acid 0.5% wt.	Air	Layering caused by increased sintering on external chip faces
Isopropanol	None	None	5 sccm Ar	Poor sintering
Isopropanol	Polyethylene Glycol 2.5% wt.	Lactic Acid 1% wt.	5 sccm Ar	Chips broke apart in furnace, not enough time for binder evaporation
Isopropanol	Polyethylene Glycol 2.5% wt.	Lactic Acid 1% wt.	5 sccm Ar	Slower rise to temperature prevented chips from breaking apart, but very little sintering occurred
Isopropanol	Polyethylene Glycol $<$1% wt.	Lactic Acid 1% wt.	5 sccm Ar	Poor sintering
Isopropanol	Polyvinyl Alcohol 3% wt.	Lactic Acid 0.5% wt.	n/a	Stuck to die press and broke
None (dry powder)	None	None	5 sccm Ar	Varied based on pressure

Table 3.2: Combinations of recipes and process gasses tested to make porous SiO_2 chips. All furnace maximum temperatures were 1100 °C for 1 hour or longer.

Binders

The binders tested were polyvinyl alcohol and polyethylene glycol and were selected based on a paper by Oliver et al. [20]. In that paper, the authors utilized polyethylene glycol (PEG) 1.5% wt. and polyvinylbutyral 5.5% wt. to act as binders and hold particles together during the sintering process. The aim of that work was to create a non-porous, bubble-free silica glass, but it was thought that the binders could work in the same fashion for this work to assist sintering. The temperature was raised slowly and held constant every 50 °C for an hour until 700 °C, at which point it was raised at 10 °C/min to 1100 °C. The resulting greens utilizing binders uniformly failed to sinter, and it was suspected that the binder prevented the beads from remaining in close enough contact during the sintering process. In the case where temperature was ramped directly to 700 °C without holding every 50 °C, some level of sintering occurred, but the chips split apart during the process.

CO_2 and Air Flows

CO_2 and air flows were also explored with the DI Water and 0.5% wt. mixtures. It was thought that the added oxygen might promote neck growth between adjacent particles during the sintering process and it was observed that sintering was greatly enhanced at the surface where the oxygen concentration was likely highest due to gas flow. However, this increased sintering at the surface lead to bowing, cracking, and layering of the chips as beads were pulled closer together in some sections of the chip and not others. Figures 3-12 and 3-13 show both SEM and optical images of these chips after this process.

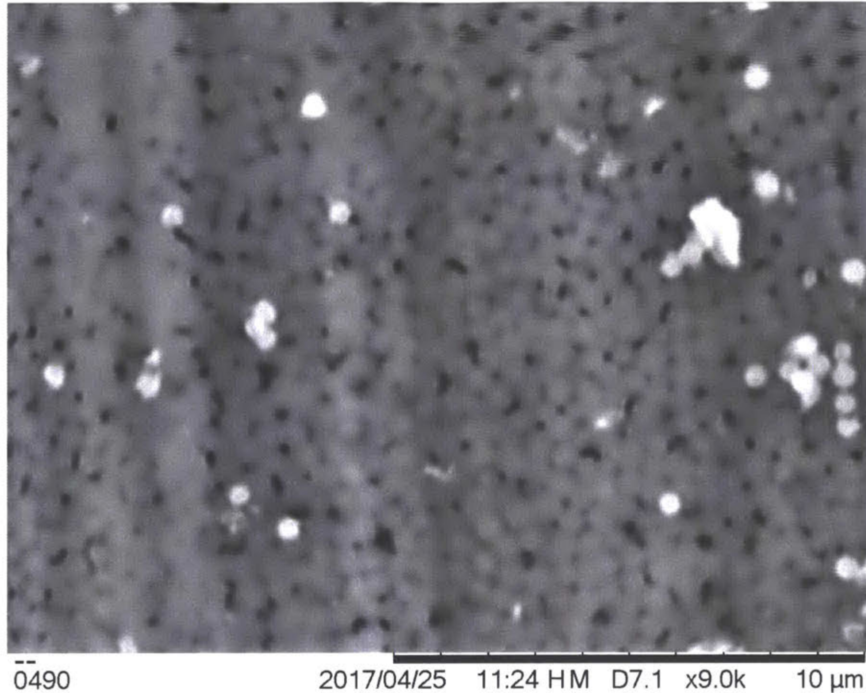

Figure 3-12: SEM of a chip surface after sintering at 1100 °C for 1 hour in 5 sccm of CO_2. Sintering was greatly enhanced; however, due to varying concentrations of oxygen throughout the chip, uneven stresses develop and result in cracking and bowing of the chip.

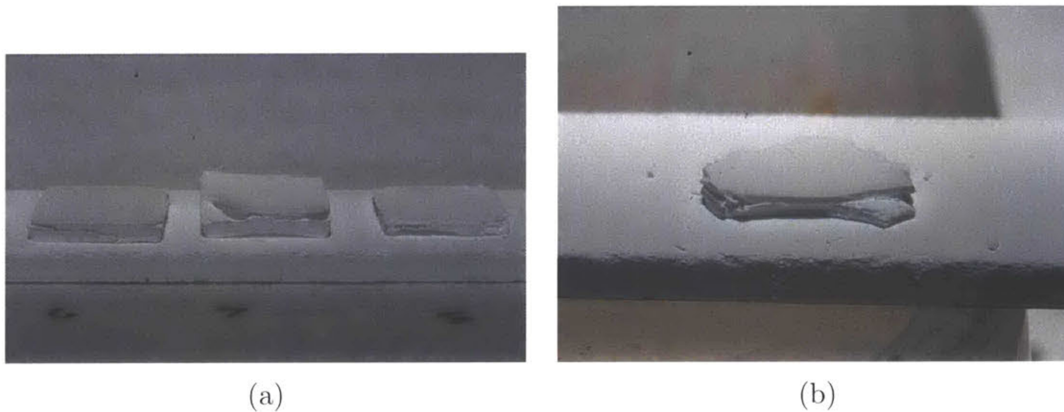

(a) (b)

Figure 3-13: Chips after sintering at 1100 °C for 1 hour in CO_2 exhibiting cracking, bowing, and layering.

Still, this is a very interesting result and if a process could be developed to ensure an even distribution of oxygen to the surface of the chip, it may be possible to lower sintering temperatures and durations as a result. This also points to potentially utilizing SiO_2 CVD processes to bind a chip by way of "growing" an SiO_2 layer around

the beads until adjacent beads are connected, potentially followed by a thermalization step. This type of CVD + thermalization process is used in MEMS fabrication to deposit SiO_2 layers greater than ~1 μm on top of Si wafers.

Isopropanol Solvent

Isopropanol was used as a solvent for a number of mixtures and has the advantage that it actively removes water from the surface of the steel die press, preventing it from rusting. Rust prevention and die press cleaning is a time-consuming additional step when working with water as a solvent, and isopropanol had the convenience of eliminating an extra cleaning step when preparing the die press after demolding a green. However, since it has a lower surface tension than water, it is less effective at holding the beads in close contact while it evaporates, and sintering performance usually suffered as a result. While most chips have unsintered sections around the edges, those produced with isopropanol as a solvent tended to crumble almost completely under normal handling.

Dry Powder

Naturally, the first attempts to create porous chips involved pressing dry powder since this offered the simplest manufacturing method. The efficacy of dry-powder pressing varied with applied pressure, which ranged from 3000 psi to 6000 psi. While some very high-quality greens were produced at 6000 psi, pressures above 3600 psi deformed the steel pressing surfaces, which manifested as non-uniform stresses in the greens and ultimately lead to consistent splitting of greens along the planar axis.

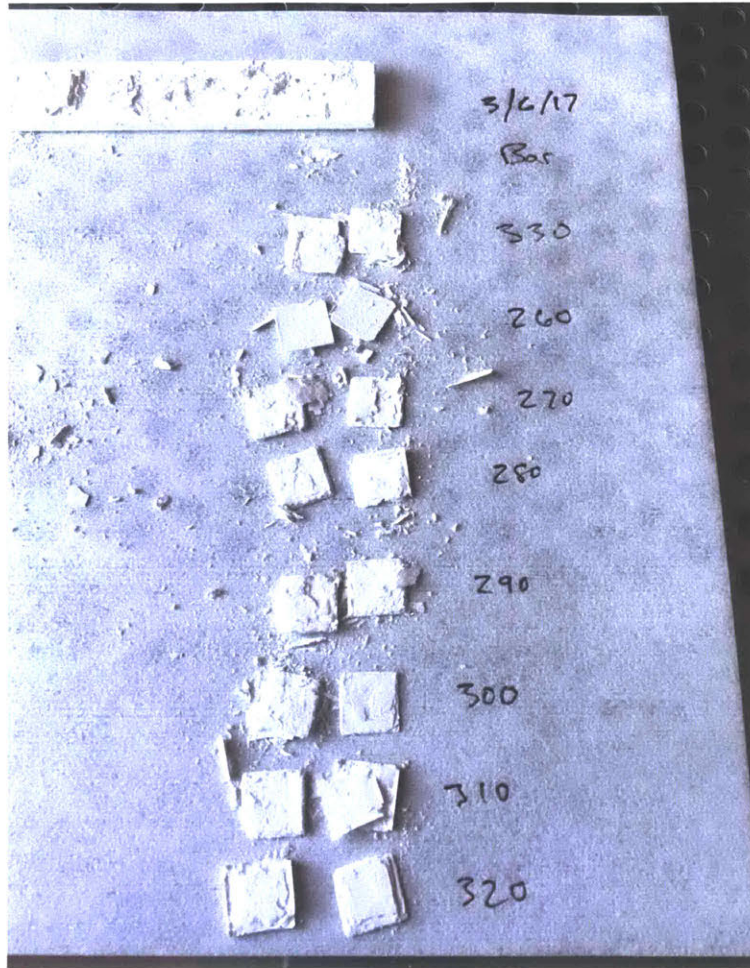

Figure 3-14: Splitting in chips as a result of die press pressing surfaces deforming from over-pressurization.

Figure 3-14 shows the result of an experiment where pressure was varied from ~3770-4800 psig (labeled 260-330 bar in the figure). This experiment indicated that the die press was being over-pressurized, and after confirming with the manufacturing company that the maximum allowable pressure for our particular die press was 3600 psig (250 bar), the pressing surfaces were re-ground and testing continued.

At pressures below ~5000 psig, dry powders tended to remain almost completely unsintered after pressing and heating in the furnace. However, higher pressures resulted in some relatively promising results. While a full chip was not successfully produced, slivers of chips pressed at 5400 psig and above exhibited strengths higher

than that of the borosilicate glass filters currently used to make emitter arrays. Figure 3-15 shows an SEM of beads pressed as a dry powder at 5400 psig.

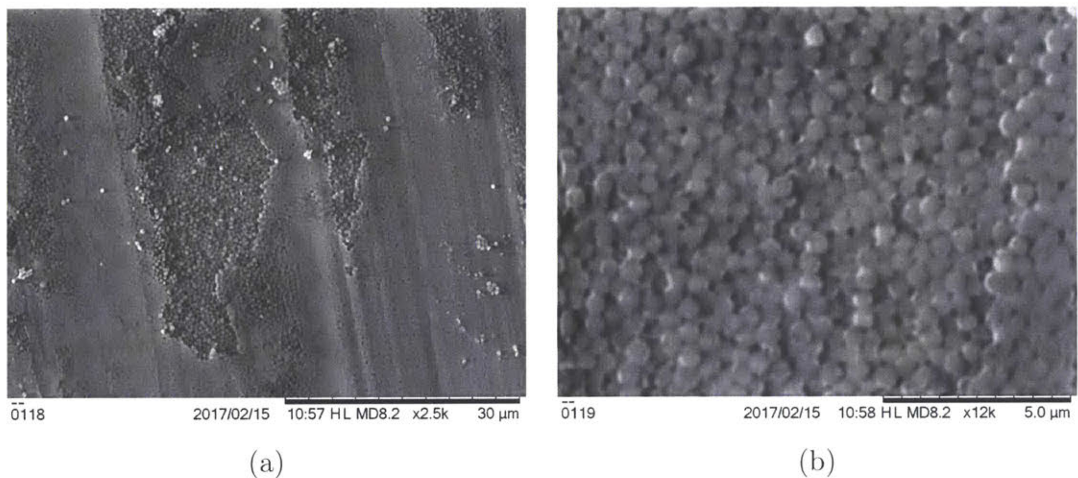

Figure 3-15: SEM of a chip after dry pressing at 5400 psig. Sintering is much more pronounced throughout the sample and in some cases has formed a solid block.

If a die press made of a stronger material than hardened steel could be found or made, it might be possible to create porous chips by simply pressing a dry powder instead of mixing in solvents or binders, and the process could potentially be simplified, though none were encountered in the course of this research.

3.3 Laser Ablation of SiO_2 Emitter Chips

3.3.1 First Laser Ablation

Laser ablation of SiO_2 chips was done at Photomachining, Inc. in Pelham, NH, using a solid-state laser with a pulse length in the picosecond range operating at 2.5 W, 500 kHz pulse rate, and 18 repetitions over the pattern. The surfaces of the chip were filed with diamond abrasive lapping pads to ensure the chip was plane parallel during ablation. The chip was made from a slurry consisting of deionized water, SiO_2 beads, and lactic acid and was pressed in the hot press at the ISN. Interestingly, this slurry mix was held at 1160 psig for 10 minutes, which typically results in layering

and splitting of chips, but in this case did not.

Due to operator error setting up the laser, the first emitters ablated into an SiO_2 emitter chip were blunt. However, this result was promising because it showed that the established process for making emitter tips could be applied to make SiO_2 emitter arrays. The chip was attached to a 3" x 1" glass microscope slide with double-sided polyimide tape. The results of this first ablation process are shown in Figure 3-16.

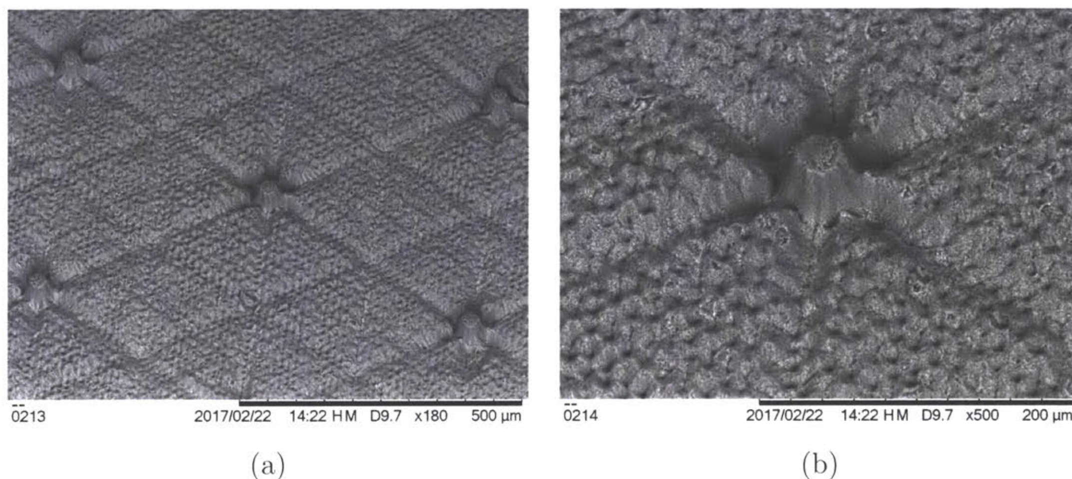

(a) (b)

Figure 3-16: SEM of the first tips laser etched into a porous chip made from sintered SiO_2 beads.

These tips are approximately 40 µm tall and have a flat top face 40 µm across. Emitters produced later had a much more typical profile (~200 µm height, height-to-base ratio of ~5:1, tip radius of 20-30 µm). This was still an extremely exciting result due to the behavior of ionic liquid in the chip. Drops of EMI-BF_4 ionic liquid were added to pieces of the chip from both the bottom as well as the patterned top side (a different piece of the chip, which broke in two during removal from the tape, was used for each method of adding ionic liquid). No pooling or flooding was seen anywhere on the chip, and it was hydrophilic enough to draw liquid into the chip, but not enough to be drawn out of patterned top surface of the chip. A comparison of the same emitter is shown in Figure 3-17.

Figures 3-18 and 3-19 further highlight the excellent performance of the chips when exposed to ionic liquid. Divots and trenches between emitters are locations

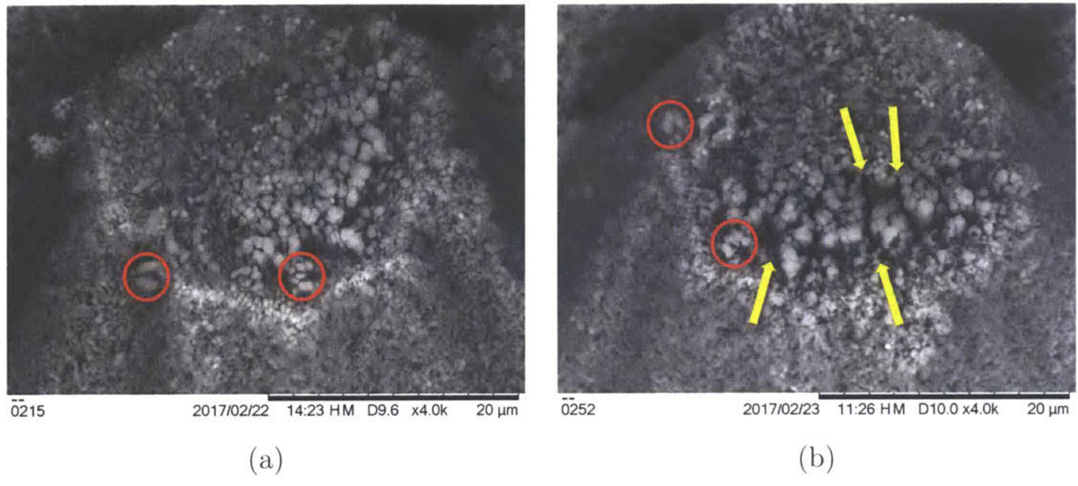

(a) (b)

Figure 3-17: The same emitter (a) with and (b) without ionic liquid. The site has been rotated just under 90° clockwise in (b) (landmark features are circled in red). Ionic liquid is visible as a slight darkening of the region between beads on the top of the emitter (yellow arrows).

where pooling typically occurs, yet in the six trenches hexagonally arranged around the emitter, no pooling occurs as seen in Figure 3-18.

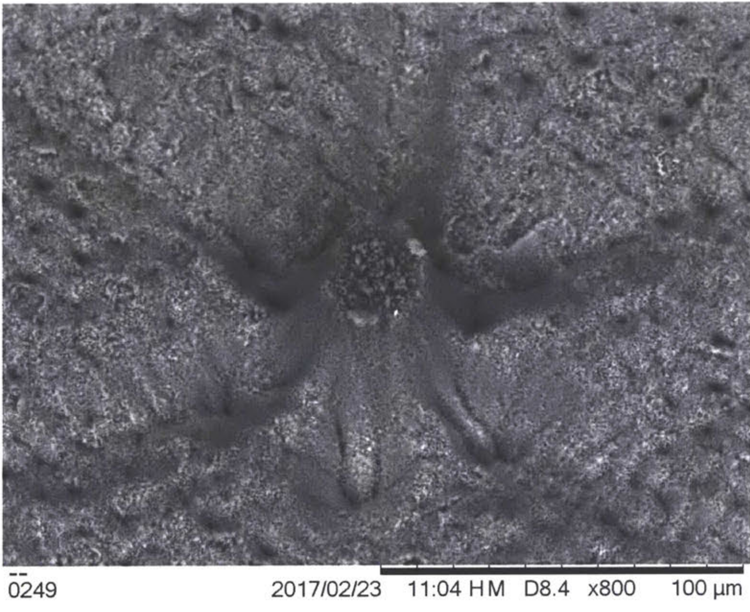

Figure 3-18: 800x SEM of SIO_2 chip with ionic liquid.

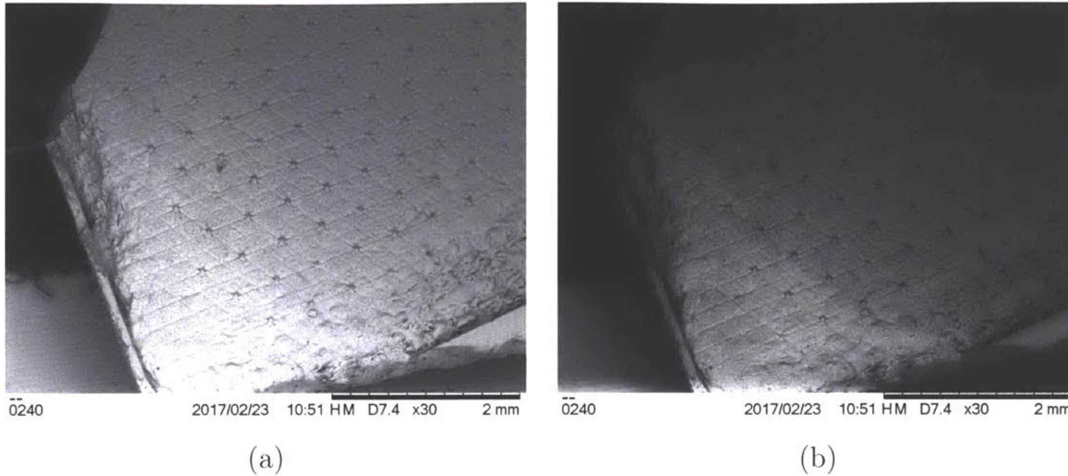

(a) (b)

Figure 3-19: A piece of the chip filled with ionic liquid from the opposite side of the chip at 30x magnification. Global adjustments to contrast, highlights, shadows, whites, blacks, and clarity were made in Adobe Lightroom CC 2015 in image (b) to better show the extent of the ionic liquid in the chip, which is visible as the circular darkened area.

3.3.2 Laser Parameter Variation for Emitter Refinement

Further tests of laser ablation were conducted to refine laser parameters and give higher quality emitters as well as to fabricate an emitter array from a chip mounted on a frame which could then be tested in a vacuum chamber. Laser power, number of repetitions, and repetition rate were varied and small 1 mm x 1 mm test patterns were etched into the chip. From the prior experiment, it was not known with certainty if the shortened, blunt emitters were due to an error in the laser parameters, or if the material simply ablated at a lower rate than borosilicate glass.

It was quickly seen that the sintered SiO_2 ablated at an almost identical rate to the borosilicate glass, and that the previous result was likely due to a failure to ensure the sample stage was set to the correct height, causing the laser to be out of focus.

The best emitters are those with the sharpest tips (lowest radius of curvature), and this is the one from Figure 3-20(b). This corresponded to a pulse repetition rate of 500 kHz, laser power of 4.5 W, and 18 passes over the grid pattern specifying the location of the emitters. The tips in this pattern had a radius of curvature of roughly

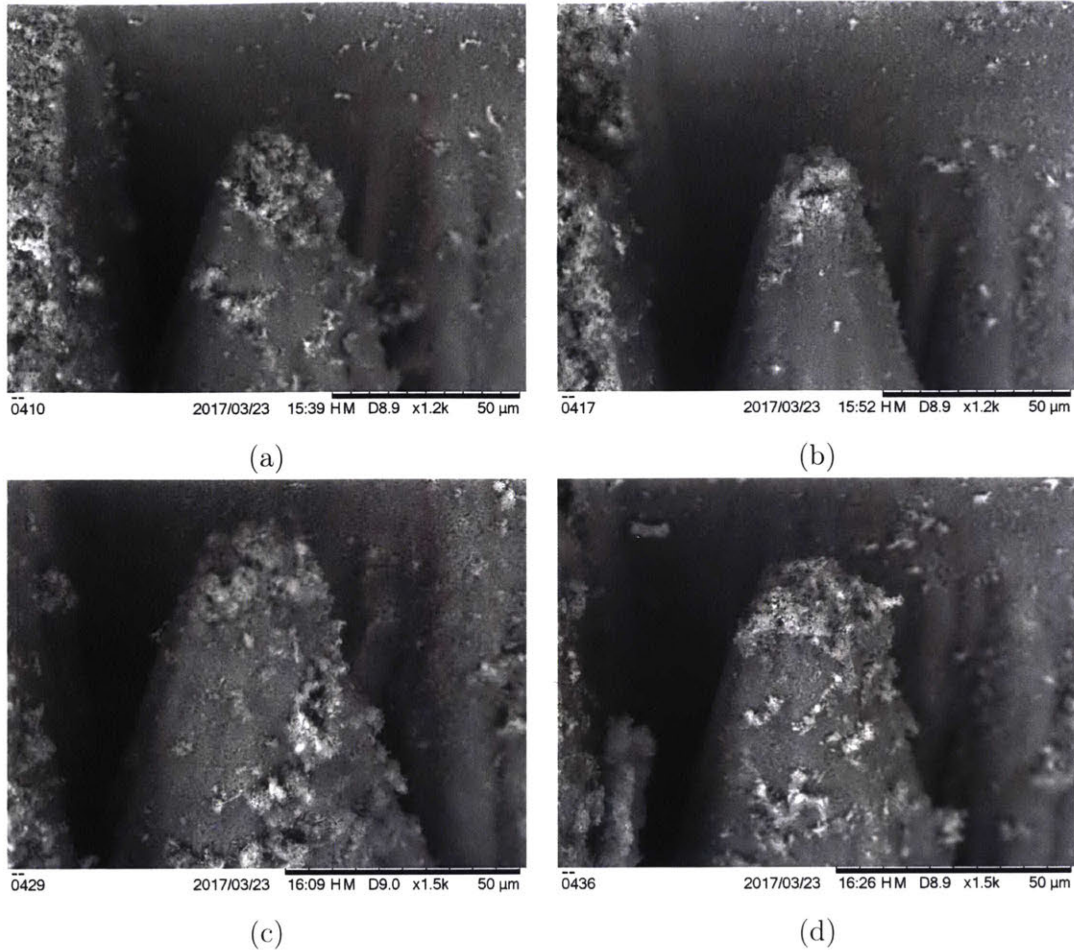

Figure 3-20: SEMs of emitters with varying laser ablation parameters. (a) 500 kHz repetition rate, 3.5 W laser power, 18 passes (b) 500 kHz repetition rate, 4.5 W laser power, 18 passes (c) 500 kHz repetition rate, 4.5 W laser power, 12 passes (d) 500 kHz repetition rate, 4.5 W laser power, 15 passes. Note that (a) and (b) are 1200x magnification while (c) and (d) are 1500x magnification. Debris on emitter tips is caused from ablated material being re-deposited during ablation process and could likely be mitigated with increased airflow.

10-15 µm compared to 20-30 µm for borosilicate emitter chips.

Full-chip patterns of 480 emitters were etched into two SiO_2 chips mounted on Si frames used in traditional iEPS packaging. To etch the pattern, a grid of lines specifying the laser path is drawn in AutoCAD. Circles marking the locations of each of the emitters indicate when the laser should turn off as it passes overhead, leaving material remaining. As material is removed, the beam becomes increasingly out of focus, which gives the emitters their conical structure. The diameter of the circles in

the grid pattern strongly affects the radius of curvature of the tips, and unfortunately the circle diameters in the 1 mm x 1 mm test pattern were 30 µm in diameter while the diameters in the full array pattern were 40 µm in diameter. The ideal diameter varies from material to material, but since the full pattern was not available with 30 µm circles, the tips in the fully etched SIO_2 array were not as sharp as the ones in the test pattern.

Figure 3-21 shows the results of the full pattern ablation. These emitters are similar in quality to that of the borosilicate glass, and the pattern used to fabricate these chips was the same AutoCAD file used for current production chips. The laser settings were 500 kHz, 3.5 W, and 18 passes over the grid pattern. This chip was subsequently filled and tested in a vacuum chamber, and the results are discussed in chapter 4.

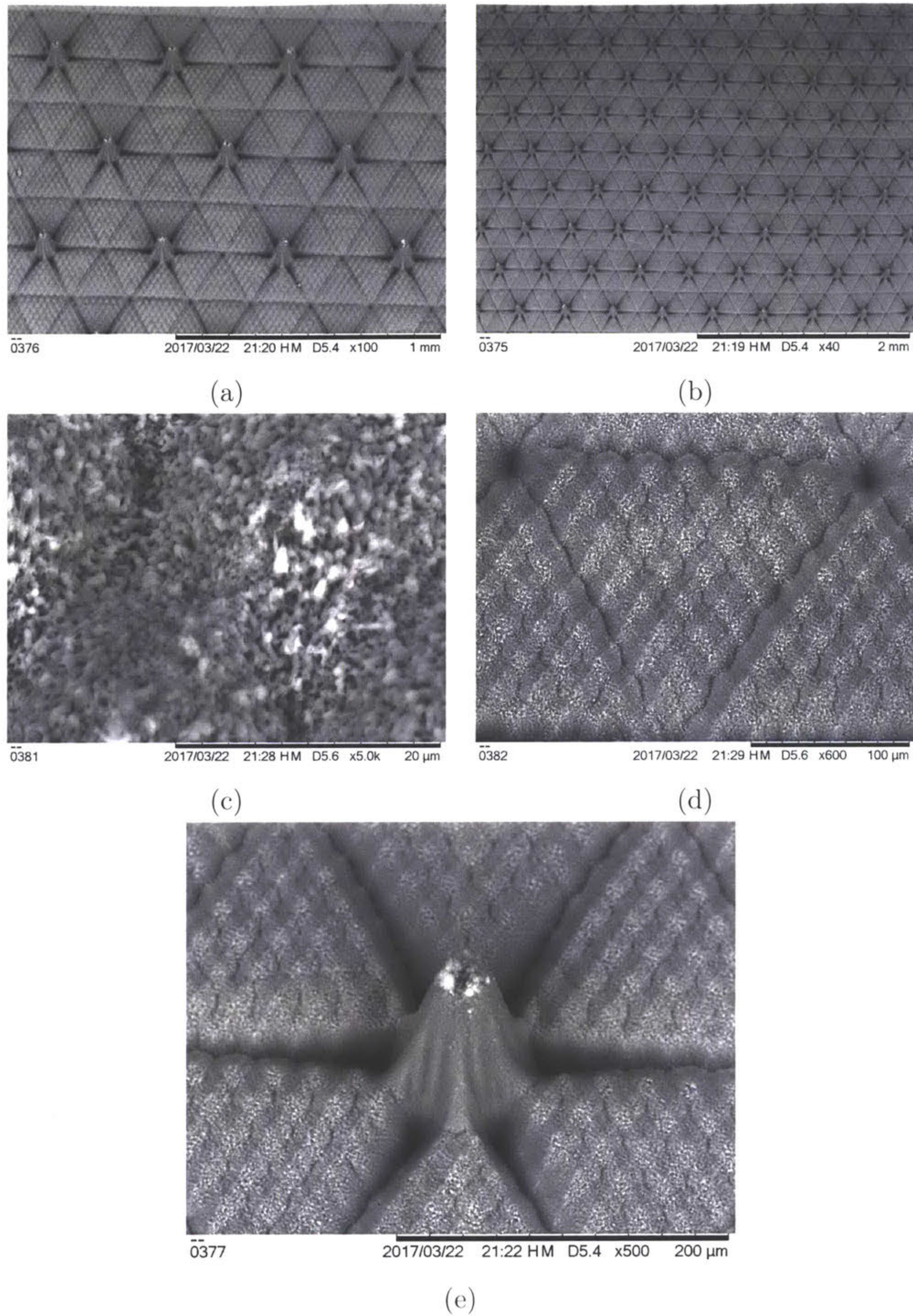

Figure 3-21: Full 480 emitter pattern in SiO_2 chip. (a) Emitter array at 100x magnification (b) 40x magnification (c) 5000x magnification of trench area between tips. Pore size is between 0.1-1 µm. (d) 600x magnification of trench area between emitters. (e) A single emitter with tip radius of curvature ~40 µm. This pattern used a larger circle to indicate a pause in the laser ablation than the test patterns in Figure 3-20 and is therefore less sharp.

Of particular note is the uniformity of the emitter array, which becomes especially apparent when compared with a recent borosilicate array as seen in Figure 3-22.

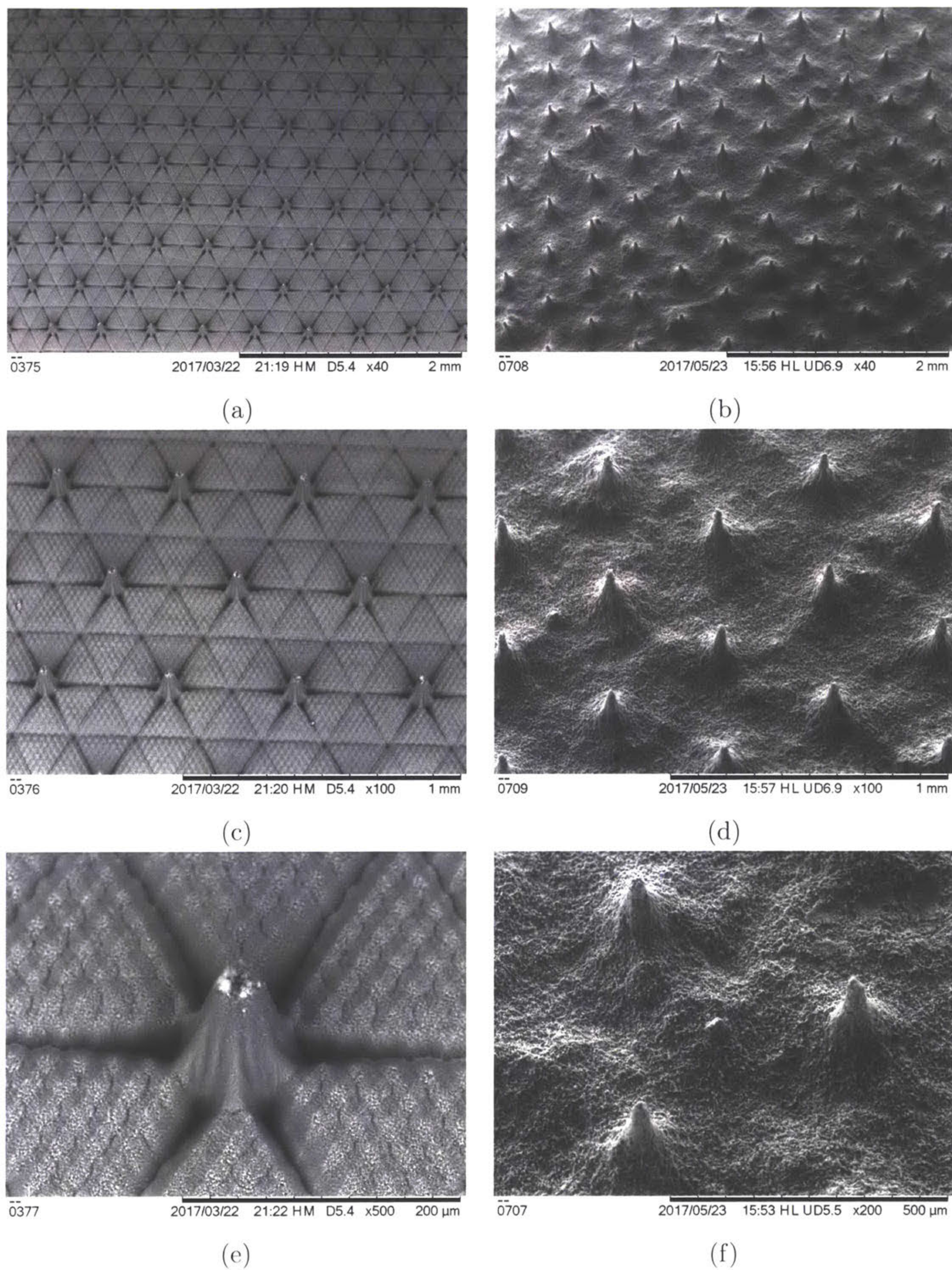

Figure 3-22: A comparison of laser-etched SiO_2 (left) and borosilicate (right) arrays.

An exciting result of this experiment is seen when adding ionic liquid to the

patterned chip. This chip was originally a full emitter chip on a frame, however the frame cracked in half during removal from the glass slide on which it was mounted. EMI-BF_4 was added to the back of the chip until it reached saturation and left for a period of two months. Figure 3-23 shows an emitter as well as a deep trench at the base of the emitter, both showing good liquid containment.

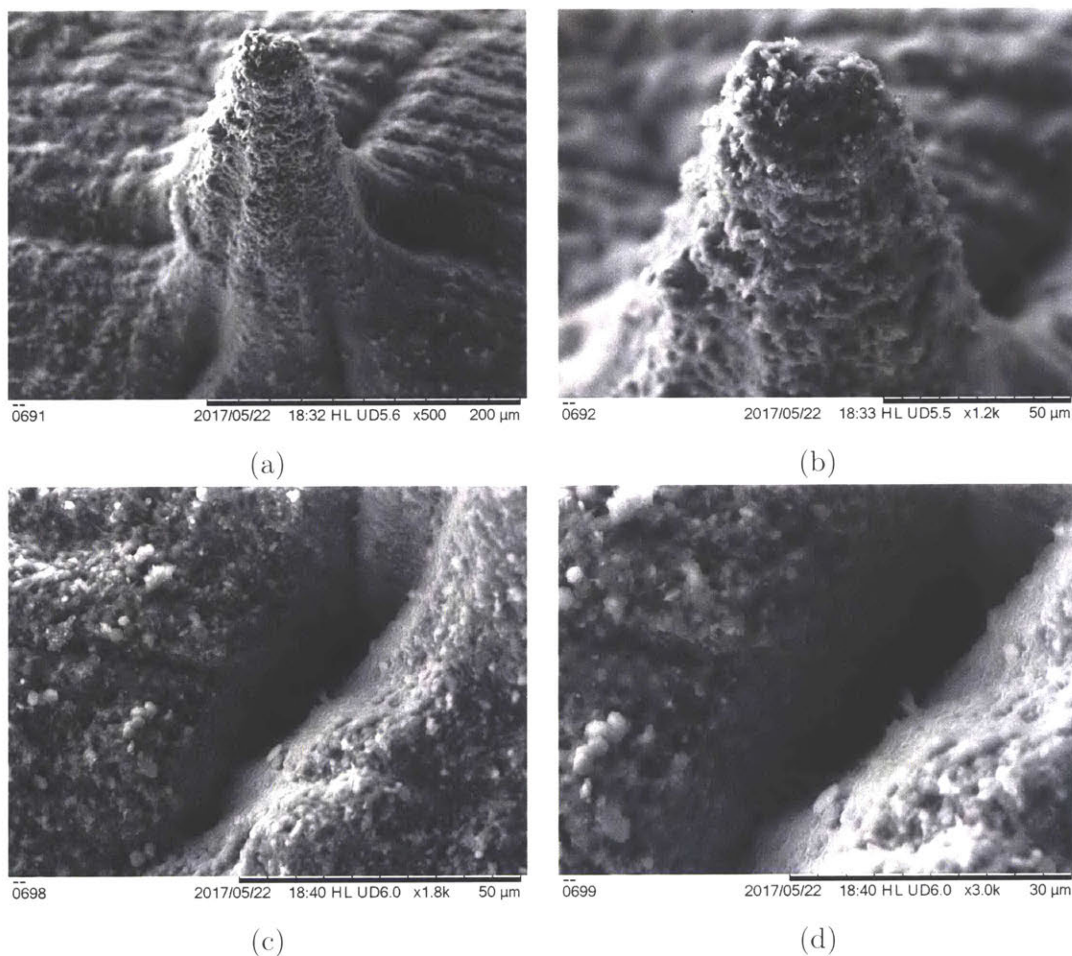

Figure 3-23: SEM of laser-etched SiO_2 saturated with ionic liquid for two months. No pooling or flooding is visible.

This is promising evidence for the idea that the smaller pore sizes could greatly reduce or eliminate the phenomenon of ionic liquid creep as described in section 3.1.

Chapter 4

Test Results

4.1 Si Mold Array

To test the finished array, the die was bonded to an existing Si frame package used for traditional iEPS thrusters and aligned to an extractor by eye. The Si was secured to the frame using a room-temperature-curing epoxy (Figure 4-1) and filled with EMI-BF_4 ionic liquid from the handle side. The tips were about 0.5 mm from the bottom plane of the extractor grid, which is a relatively large value. From electrospray theory, it can be shown that the expected voltage required to initiate emission from a tip is

$$V_{start} = \sqrt{\frac{\gamma R_c}{\epsilon_0}} ln\left(\frac{4d}{R_c}\right) \tag{4.1}$$

where R_c is tip radius, d is distance between emitter tip and extractor, γ is ionic liquid surface tension, and ϵ_0 is the permittivity of vacuum. For R_c = 50 μm, d = 0.5 mm, and γ = 0.05 N/m, we get a V_{start} = 2329 V.

Arrays were tested in an SPL vacuum chamber at pressures of roughly $5e^{-6}$ Torr. The vacuum chamber was a 1' x 2.5' stainless steel chamber with both roughing and

turbo pumps and ion gauge for measuring low pressure. The array was electrically connected to a voltage source capable of outputting -2.5 kV to 2.5 kV. An extractor grid was mounted above the array (Figure 4-2) and connected to earth ground.

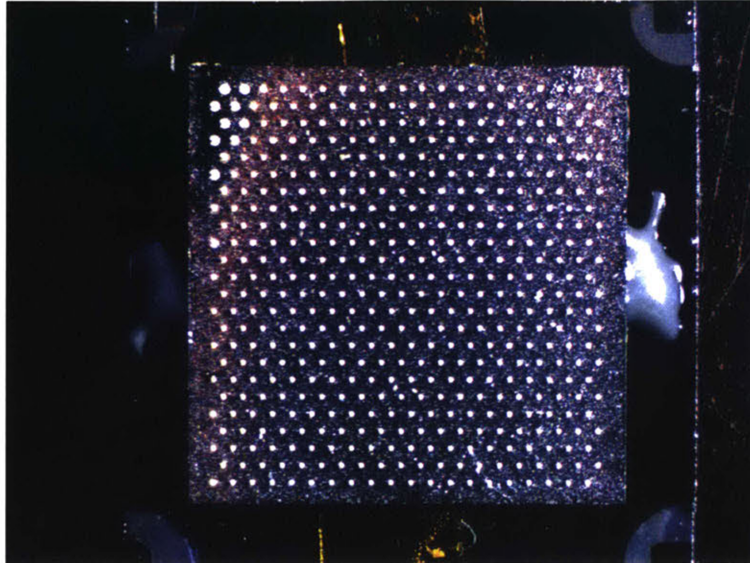

Figure 4-1: Soda-lime glass array in Si mold.

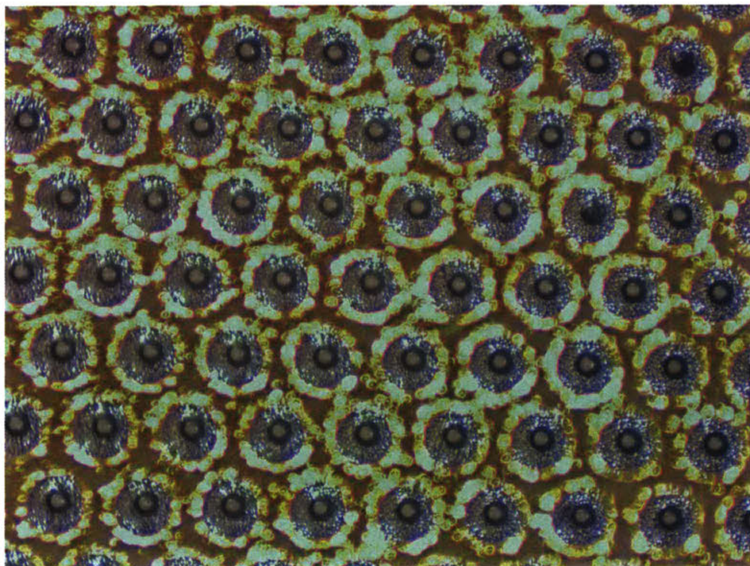

Figure 4-2: Molded soda-lime glass array seen through extractor.

4.1.1 Current vs. Voltage Plot

After "warming up" the thruster to get a sense of characteristic voltages and currents, a plot of current vs. voltage was generated by linearly ramping the voltage from 0 to +/-2250 while recording current drawn by the power supply (Figure 4-3). The voltage required to initiate emission was about 2000 V (and is similar to the value calculated from equation 4.1) and the voltage was raised to an absolute magnitude of 2250 V in both positive and negative polarities.

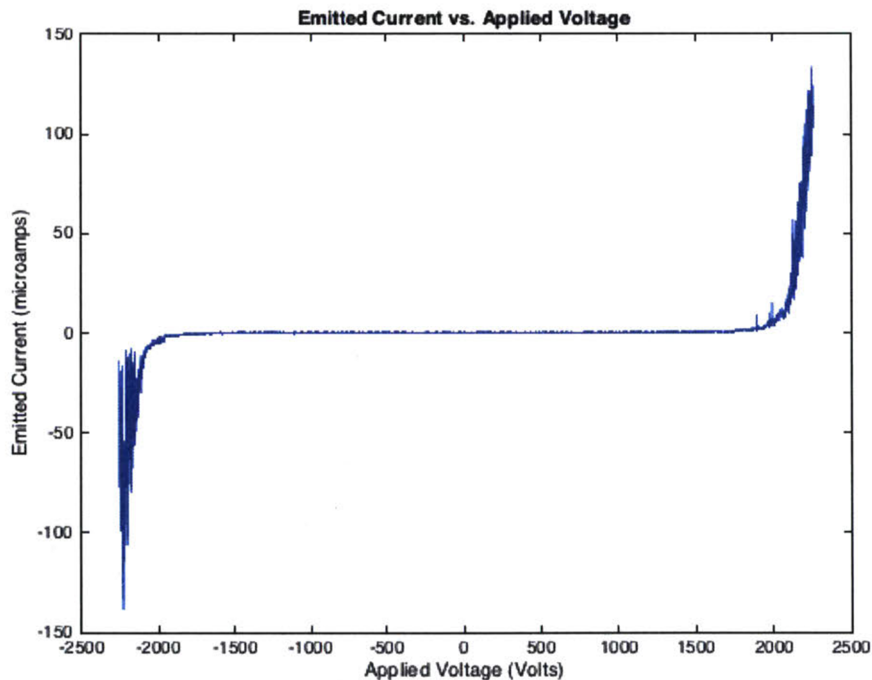

Figure 4-3: Voltage vs. current from molded soda-lime glass array.

A typical value for borosilicate iEPS emitters is 800 V, so these firing voltages are around 1200-1400 V higher than a normal thruster. Reducing distance from tip to extractor grid as well as tip radius will decrease this start up voltage further, and could potentially be reduced to similar values for borosilicate emitter arrays.

4.1.2 Trapezoidal Voltage Waveform

An alternating trapezoidal voltage waveform was also applied, which simulates the thruster operational mode on a satellite in order to prevent charge buildup.

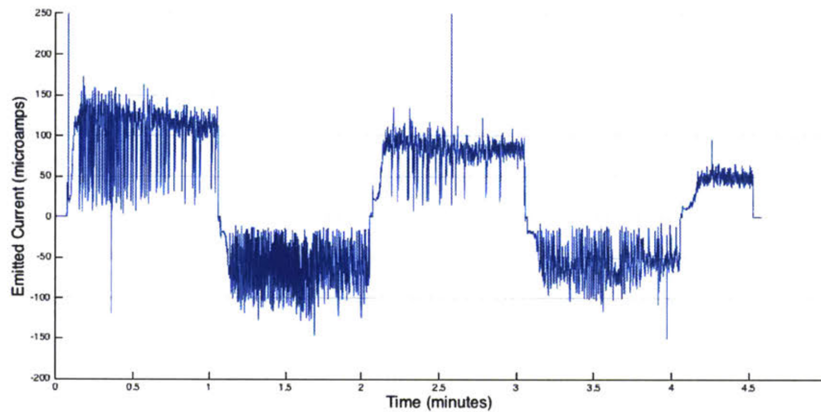

Figure 4-4: Emitted current from molded soda-lime glass array.

Emitted current reached almost 150 μA at approximately +/-2250 V, and emission was more stable in the positive mode than the negative mode. Because of a slight offset in the software, the negative mode, while commanded to 2250 V, applied a slightly lower voltage resulting in less average current than in the positive mode. This result is the first instance of electrospray emission from a porous array of tips created in a mold made using MEMS processing technology.

4.2 SiO_2 Nano-Bead Array

The patterned emitter created during the results of section 4.2 was filled with 1-Ethyl-3-methylimidazolium bis(trifluoromethanesulfonyl)imide (EMI-Im) tested in an SPL vacuum chamber at approximately 5e^{-6} Torr. Measurements including retarding potential analysis (RPA), current vs. voltage, and trapezoidal waveform were performed.

4.2.1 Current vs. Voltage Plot

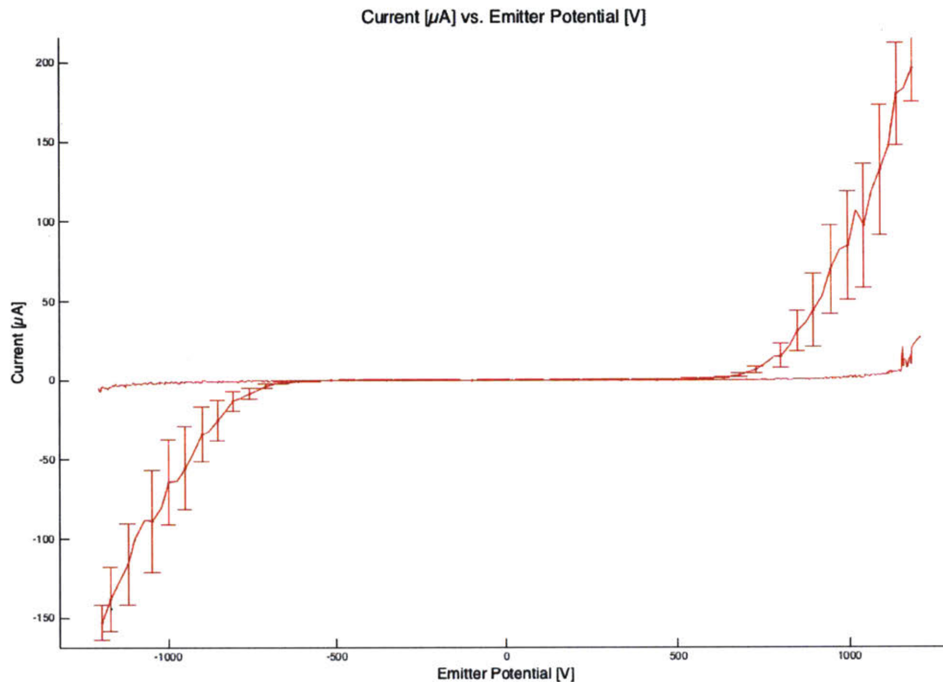

Figure 4-5: Current (μA) vs. voltage (V) for SiO_2 array on a temporary mount. The flatter line is current intercepted by the extractor grid.

Emission begins at around +/-460 V and is especially low due to the low surface tension of EMI-Im. Current reaches -150 μA at -1250 V in the negative mode and approximately 180 μA at 1250 V in the positive mode. This is similar to presently fabricated borosilicate emitters and could likely be greatly improved by implementing a full array of tips seen in Figure 3-20b. Intercepted current, which is current drawn by the extractor and caused by ions impacting the extractor and failing to escape, is shown as the flatter red line in Figure 4-5 and was under 3% of emitted current (discounting some noisier emission in the high end of the positive mode). This is a strong result on par with some of the best emitters tested in the SPL.

4.2.2 Retarding Potential Analysis

A retarding potential analyzer (RPA) is a device used to measure the degree of fragmentation in an ion beam. An iEPS device can operate in a number of emission modes; the pure ionic regime where single ions leave the Taylor cone without carrying neutral cation-anion pairs with them, the solvated ion mode where emitted ions carry one or more neutral cation-anion pairs with them, or the droplet mode, where droplets consisting of sometimes thousands of neutral pairs are emitted with tens of cations or anions. When solvated ions are emitted, the neutral pairs can fragment, which reduces the mass of the accelerated ion. If this happens before the ion has left the acceleration region, it will have a lower velocity than had there been no fragmentation, and it will therefore require less voltage to fully stop the ion. If the ion beam is directed at a Faraday cup to measure collected current and a biased grid is placed in front of the Faraday cup, the voltage of the biased grid can be varied from zero to the thruster accelerating voltage, and the resulting curve will give information about the makeup of the beam. A diagram of an RPA is shown in Figure 4-6.

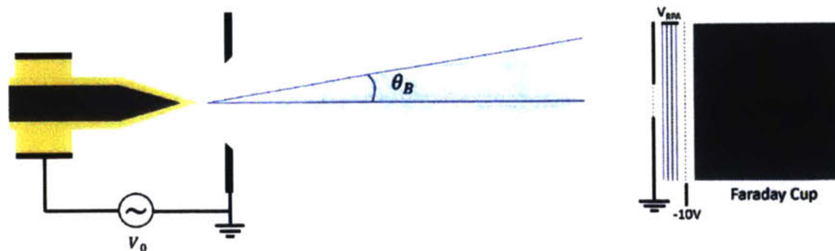

Figure 4-6: Diagram of a retarding potential anaylzer. [21]

The best case from an efficiency standpoint is one in which all of the emitted ions leave individually without any neutral pairs tagging along. In such a case, the current measurement from the Faraday cup would be constant until the biased grid voltage equals that of the thruster and would look like the graph in Figure 4-7.

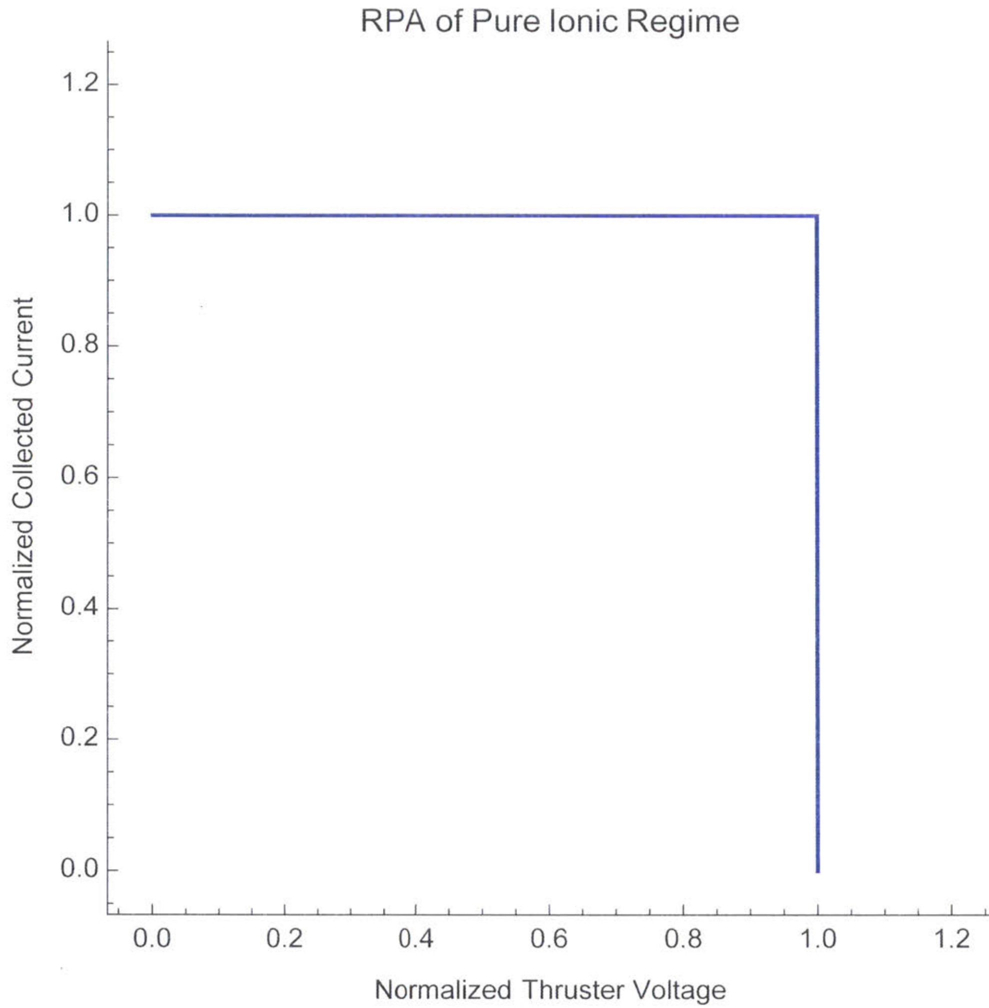

Figure 4-7: RPA output for pure ionic regime with no fragmentation in the acceleration region.

Fragmenting ions will appear as a partial decay in collected current, and an idealized case is shown in Figure 4-8.

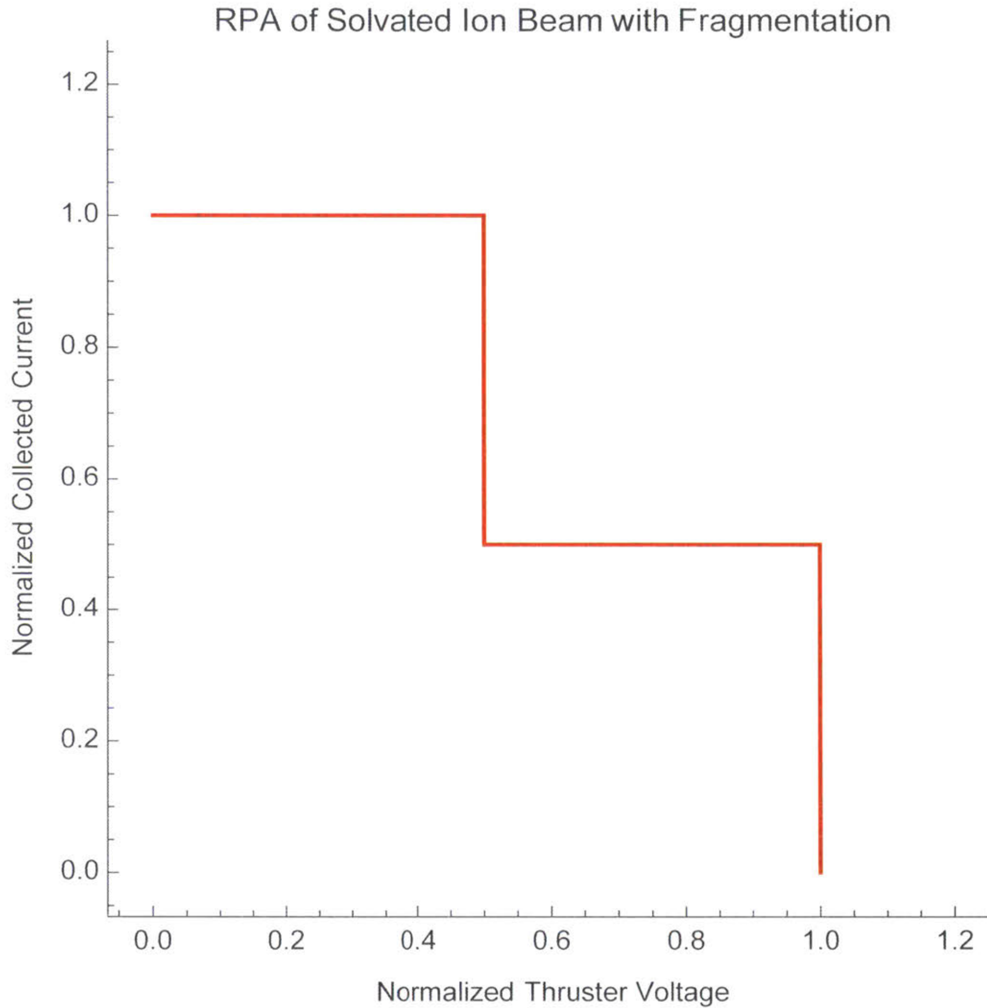

Figure 4-8: RPA output in the event of 50% fragmentation of a single species of solvated ions.

In the actual test, the data show an fairly linear decrease, which is indicative of a large amount of fragmentation happening throughout the acceleration region, as well as a wide range of solvated ions and droplets being emitted. However, this conclusion requires time-of-flight spectroscopy to confirm. This is not ideal; however this is due in large part to the use of EMI-Im and would also be improved by increased emission tip sharpness. This plot is shown in Figure 4-9.

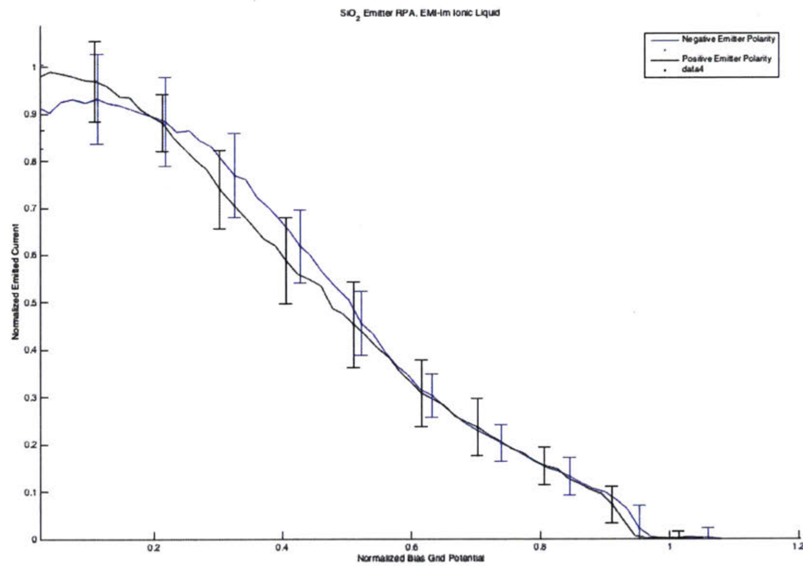

Figure 4-9: RPA output SiO_2 emitter array filled with EMI-Im.

4.2.3 Trapezoidal Voltage Waveform

Lastly, to get a sense of how the thruster would behave under operational conditions similar to long-duration operation, a trapezoidal waveform was applied whereby the voltage is alternated from positive to negative with a 30-second period. In practice this is to help prevent electrochemistry in the distal electrode. The output of the test is shown in Figure 4-10.

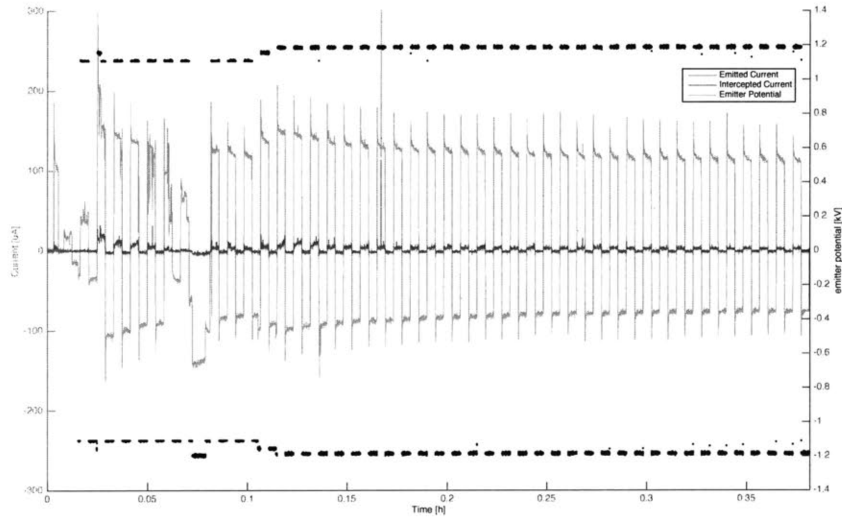

Figure 4-10: Trapezoidal voltage waveform applied to SiO_2 emitter for approximately 24 minutes.

The thruster was fired with this waveform for approximately 24 minutes. The thruster was operated at 1125 V for just over six minutes before the voltage was increased to 1175 V for the remainder of the test. The voltage was selected to initially give an emitted current of 150 µA in the positive mode, though emitted current eventually fell to a steadier value of roughly 115 µA in the positive mode and roughly 95 µA in the negative mode. Intercepted current, which is current drawn by the extractor and is caused by ions impacting the extractor and failing to escape, was approximately 5% of emitted current or less, and could likely be improved with sharper emission tips and different ionic liquids.

Chapter 5

Summary and Future Research Directions

With small satellites becoming cheaper and more accessible, a clear need for a propulsion system able to meet an extremely stringent set of design requirements has emerged. Reducing thruster size while maintaining efficiency, thrust density, reliability, and cost effectiveness has proven to be a unique challenge, which few existing propulsion technologies are able to solve. iEPS has shown great potential to be able to solve this problem, although significant design challenges remain. iEPS area thrust densities are around two orders of magnitude lower than ion engines and Hall thrusters, two of the more widely-used electric propulsion thrusters. For iEPS to become competitive with these types of propulsion systems, emitter array pitch must be decreased by a factor of 5-10. To accomplish this, new fabrication methods must be explored and developed. Limitations in subtractive processing mean alternative, nano-scale fabrication methods such as those utilized in MEMS processing provide the most promise towards achieving increased thrust densities.

Thruster lifetime is most often limited by propellant containment issues, and for iEPS to compete with other electric propulsion technologies, advancements in

materials must be made. Propellant containment issues manifest in a number of ways. They can be caused by a slow buildup of liquid in the trenches between emitters in an iEPS emitter array, eventually increasing enough to make contact between the propellant and ion extractor grid, short circuiting the thruster. They can also manifest as a propellant "creep" phenomenon where ionic liquid moves along the Si frame, to the insulating corner posts, and bridges the insulating glass layer, which also short circuits the thruster.

Solving this problem with hydrophobic surface coatings without adversely impacting thruster performance and reliability is difficult. A more ideal solution is to fabricate emitter arrays with smaller, more uniform pores and features to address this issue without adding the additional complexity of coatings.

This work has made a number of advancements on both fronts, and lays a clear and exciting path forward for iEPS emitter development. First, it has built on the work by Xie in her Master's thesis and created an array of molded porous emitters using MEMS fabrication methods. One such array was filled with ionic liquid and fired.

A process for manufacturing uniform porous substrates by the process of sintering SiO_2 nano-beads in a laboratory table-top furnace was also developed. This work demonstrates a number of characteristics of SiO_2 emitters, which show great promise in solving some of the main issues seen with current borosilicate emitter arrays.

5.1 Array Molding

A MEMS process for batch creation of 1 cm x 1 cm Si molds was successfully designed and implemented. This process utilized standard MEMS processing techniques and should be readily implemented in any standard MEMS facility. The resulting wafers contained 109 molds in a range of pitches and emitter diameters. A range of materials

for the creation of porous emitter arrays was explored, and it was determined that micro- and nano-beads showed the most promise for reliably creating emitters. In addition, this work demonstrated the importance of uniformity in the size of micro- and nano-beads.

A molded emitter array was successfully fabricated and tested in an SPL vacuum chamber. This array successfully emitted over 100 µA of current at +/-2250 V using EMI-BF_4 ionic liquid propellant, which is a typical value for emitted current in a state-of-the-art iEPS thruster.

This manufacturing method also successfully demonstrated the viability of using MEMS processing to decrease emitter pitch by at least a factor of two. Further decrements in pitch should be readily achievable utilizing the same manufacturing method outlined in this work.

5.2 SiO_2 Emitter Arrays

A process for creating 1 cm x 1 cm x 1 mm porous chips via hydraulic pressing and subsequent sintering in a tabletop furnace was successfully developed. Highly-uniform SiO_2 beads of 750 nm diameter were pressed in a hardened-steel die press using water-based mixtures, forming green bodies, which were then sintered at 1100 °C for 1-2 hours. The resulting porous chips showed excellent uniformity and ionic liquid containment properties.

Laser ablation tests demonstrated remarkably uniform emitter arrays and indicate that this material has the potential to outperform borosilicate emitter arrays in ablation uniformity, emitter tip sharpness, and post-ablation ionic liquid containment. This work highlights the potential for SiO_2 emitters to operate without surface coatings, both due to the smaller and more uniform pore size than that of the borosilicate glass as well as due to the physics of microfluidics in an array of adjacent spheres.

A fully-functional emitter array on a Si frame was created and tested in the SPL. This thruster used EMI-Im ionic liquid, and current vs. voltage emission characterization, retarding potential analysis, and voltage waveform emission characterization was done. The results indicate that this material has a very strong potential to replace borosilicate glass as the principal material for iEPS emitter arrays.

5.3 Future Research Directions

5.3.1 Array Molding

This work showed the feasibility of creating iEPS emitter arrays using MEMS processing techniques. One of the main drawbacks to using this technique was the narrow range of available materials compatible with the Si molds and subsequent sintering and RIE processing. Many deep reactive-ion etching machines have much better Si:SiO_2 selectivity ratios – on the order of 50:1 or 100+:1 instead of the 3:1 available in the MIT EML. Though these machines exist in the MTL, they are generally not available for use with our processes due to stringent machine particulate and contamination restrictions.

If a facility could be found that would allow the process developed in this work to be used in a machine with higher Si:SiO_2 selectivity, then the two manufacturing methods examined here could potentially be combined in order to create molded SiO_2 emitter arrays. The small degree of SiO_2 etching that would occur would actually be a benefit, since the flat top of the emitters produced in this work have drawbacks to emitter performance.

Similarly, if a source of monodisperse soda-lime nano- or micro-beads could be found, they could potentially be used more reliably to create molded emitter arrays. Such a material could also be used in the same process developed for making SiO_2 emitter arrays.

5.3.2 SiO_2 Emitter Arrays

Multiple improvements to the state of the art were made during the course of this work, including sharper emitter tips, improved ionic liquid containment, and improved material uniformity. The combination of all of these in a single emitter array was not achieved due to time constraints; however, few obstacles exist to the creation of such an array. Implementing an array of sharper tips is only a matter of developing the correct laser pattern. The use of EMI-Im in the fired array was due to limited available ionic liquid selection, but an extensive variety of ionic liquids exist, many of which have more desirable intrinsic properties.

This work also lacked access to a furnace capable of reaching temperatures higher than 1100 °C, but such furnaces exist even in a tabletop package. Sintering at higher temperatures could greatly increase yield from the hydraulic pressing process, allow for lower pressing forces, and reduce the need for complicated mixtures or potentially even allow for dry-powder sintering. Furthermore, higher sintering temperatures could potentially allow for the development of highly-controlled mixtures of bidisperse SiO_2 particle sizes, which could facilitate the use of smaller beads as a glue for the larger beads in a way which was not available with the soda-lime glass used in the array molding work.

5.4 Conclusion

This work has provided an exciting avenue forward for the improvement of iEPS through the implementation of advanced materials and manufacturing processes. These show the potential to solve some of the most pressing challenges in iEPS thruster implementation, and could allow for iEPS to become a viable alternative to existing electric propulsion systems for the most advanced and technologically demanding space missions.

Bibliography

[1] Paulo C. Lozano. Lecture Notes, 16.522: Space Propulsion Lecture 1, February 2016.

[2] https://sec353ext.jpl.nasa.gov/ep/img/nexis_ion_thruster.jpg. JPL's NEXIS ion thruster.

[3] https://sec353ext.jpl.nasa.gov/ep/img/hall_thrusters/bht8000_175_8kw_200v.jpg. Busek BHT-8000 Hall thruster.

[4] Zhigang Zak Fang and R. M. German. *Sintering of advanced materials: Fundamentals and processes*, chapter 1.3. Woodhead Publishing Limited, 2010.

[5] Tom Benson. Brief History of Rockets. https://www.grc.nasa.gov/www/k-12/TRC/Rockets/history_of_rockets.html, June 2014.

[6] NASA, The Boeing Company, McDonnell Douglas Astronautics Company, International Business Machines Corporation, and North American Rockwell Corporation. Saturn V News Reference. Technical report, 1967.

[7] G.I. Taylor. Disintegration of water drops in an electric field. *Proceedings of the Royal Society of London. Series A, Mathematical and Physical Sciences*, 280(1382):383–397, 1964.

[8] Robert S Legge Jr. *Fabrication and characterization of porous metal emitters for electrospray applications.* PhD thesis, Massachusetts Institute of Technology, 2008.

[9] Daniel George Courtney. *Ionic liquid ion source emitter arrays fabricated on bulk porous substrates for spacecraft propulsion.* PhD thesis, Massachusetts Institute of Technology, 2011.

[10] Louis Evan Perna. Design and manufacturing of an ion electrospray propulsion system package and passively-fed propellant supply. Master's thesis, Massachusetts Institute of Technology, 2014.

[11] Steven Mark Arestie. Porous material and process development for electrospray propulsion applications. Master's thesis, Massachusetts Institute of Technology, 2014.

[12] Natalya Brikner and Paulo C. Lozano. The role of upstream distal electrodes in mitigating electrochemical degradation of ionic liquid ion sources. *Applied Physics Letters*, 101(19):193504, 2012.

[13] Chase Coffman, Manuel Martinez-Sanchez, F.J. Higuera, and Paulo C. Lozano. Structure of the menisci of leaky dielectric liquids during electrically-assisted evaporation of ions. *Applied Physics Letters*, 109(23), 2016.

[14] F. de la Mora and I.G. Loscertales. The current emitted by highly conducting taylor cones. *Journal of Fluid Mechanics*, 260:155–184, 1994.

[15] D. Krejci, F. Mier-Hicks, R. Thomas, T. Haag, and P. Lozano. Emission characteristics of passively fed electrospray microthrusters with propellant reservoirs. *Journal of Spacecraft and Rockets*, 54(2):447–458, 2017.

[16] Julie Xie. Fabrication and characterization of sintered porous glass emitters for electrospray propulsion. Master's thesis, Massachusetts Institute of Technology, 2014.

[17] Jimmy A Rojas-Herrera and Paulo C. Lozano. Mitigation of anomalous expansion of carbon xerogels and controllability of mean-pore-size by changes in mold geometry. *Journal of Non-Crystalline Solids*, 458:22–27, 2017.

[18] Iulia Jivanescu. Structure and performance of carbon xerogel molded emitters for micropropulsion applications. Master's thesis, Massachusetts Institute of Technology, 2016.

[19] Jinye Niu, Zhiwei Chen, Liu Feng, Zhengmin Li, and Min Tan. Preparation and characterization of fused silica micro-powders and ceramics. *Advanced Materials Research*, 412:315–320, 2013.

[20] C.J.R. Gonzalez Oliver, H. Tippmann, D. Richon, T. Serita, and M. Yoshioka. Sintering of silica compacts from powders obtained by atomization of organometallic solutions. *Boletin de la Sociedad Española de Cerámica y Vidrio*, 30(4):245–249, 1991.

[21] Catherine Elizabeth Miller. On the stability of complex ions in ionic liquid ion sources. Master's thesis, Massachusetts Institute of Technology, 2015.